Performance Analysis of Penta-Graphene Based Thermoelectric Generator: A Simulation Study

Mulgeta Girma Abuche

A Thesis Submitted to the Department of Applied Physics
School of Applied Natural Science

Presented in Partial Fulfillment of the Requirement for the Degree of
Master's of Science in Applied Physics (Statistical Physics)

Office of Graduate Studies

Adama Science and Technology University

June, 2024
Adama, Ethiopia

Performance Analysis of Penta-Graphene Based Thermoelectric Generator: A Simulation Study

Mulgeta Girma Abuche

Advisor: Dr. Kumneger Tadele (PhD)
Co-Advisor: Dr. Seyfan Kelil (PhD)

A Thesis Submitted to the Department of Applied Physics
School of Applied Natural Science

Presented in Partial Fulfillment of the Requirement for the Degree of
Master's of Science in Applied Physics (Statistical Physics)

Office of Graduate Studies

Adama Science and Technology University

June, 2024
Adama, Ethiopia

Declaration

I hereby declare that this Master Thesis entitled **"Performance Analysis of Penta-Graphene Based Thermoelectric Generator: A Simulation Study"** is my original work. That is, it has not been submitted for the award of any academic degree, diploma or certificate in any other university. All sources of materials that are used for this thesis have been duly acknowledged through citation.

Name of student	Signature	Date

Recommendation

We, the advisors of this thesis, hereby certify that we have read the revised version of the thesis entitled **"Performance Analysis of Penta-Graphene Based Thermoelectric Generator: A Simulation Study"** prepared under our guidance by Mulgeta Girma submitted in partial fulfillment of the requirements for the degree of Mater's of Science in Applied Physics (Statistical Physics). Therefore, we recommend the submission of revised version of the thesis to the department following the applicable procedures.

Advisor	Signature	Date
Co-Advisor	Signature	Date

Approval page

We, the advisors of the thesis entitled **"Performance Analysis of Penta-Graphene Based Thermoelectric Generator: A Simulation Study"** and developed by Mulgeta Girma, hereby certify that the recommendation and suggestions made by the board of examiners are appropriately incorporated into the final version of the thesis.

Advisor	Signature	Date
Co-Advisor	Signature	Date

We, the undersigned, members of the Board of Examiners of the thesis by Mulgeta Girma have read and evaluated the thesis entitled **"Performance Analysis of Penta-Graphene Based Thermoelectric Generator: A Simulation Study"** and examined the candidate during open defense. This is, therefore, to certify that the thesis is accepted for partial fulfillment of the requirement of the degree of Master's of Science in Applied Physics (Statistical Physics).

Chairperson	Signature	Date
Internal Examiner	Signature	Date
External Examiner	Signature	Date

Final approval and acceptance of the thesis is contingent upon submission of its final copy to the Office of Postgraduate Studies (OPGS) through the Department Graduate Council (DGC) and School Graduate Committee (SGC).

Department Head	Signature	Date
School Dean	Signature	Date
Office of Postgraduate Studies, Dean	Signature	Date

Acknowledgement

Above all, I would like to thank "Almighty God," for granting me the privilege to further my education in graduate studies and for being a constant source of strength during challenging times. Additionally, I extend my heartfelt gratitude to my advisor, Dr. Kumneger Tadele (PhD), for his invaluable guidance, patient teaching and unwavering support. His mentorship has not only helped me academically but has also significantly contributed to my personal growth and success. I also express my appreciation to my co-advisor, Dr. Seyfan Kelil (PhD), for taking the time to read and comment on this research paper. Furthermore, I recognize the contributions of Mr. Tadesse Lemma, a Ph.D. candidate in Material Physics, for his guidance and mentorship during my thesis work. Moreover, I am grateful to all my instructors for sharing their knowledge and expertise in their respective fields. I also express my gratitude to the incredible individuals I have had the opportunity to collaborate with at Adama Science and Technology University. Special thanks to my parents for their unconditional love, care, support and the sacrifices they have made for my education and well-being. Their unwavering presence has been a constant inspiration in my life. Additionally, I would like to thank my friends who have supported and encouraged me throughout this journey. Lastly, I extend my sincere thanks to the Department of Applied Physics at Adama Science and Technology University for enabling me to pursue my MSc. in Applied Physics and to Madda Walabu University for providing the funding that allowed me to successfully complete my research.

Table of Contents

Declaration i

Recommendation ii

Approval Page iii

Acknowledgement v

List of Tables viii

List of figures ix

List of Acronyms and Abbreviations x

Abstract xi

1 INTRODUCTION **1**

1.1 Background of the study 1

1.2 Statement of the problem 2

1.3 Objectives 3

1.3.1 General objective 3

1.3.2 Specific objectives 3

1.4 Significance of the study 3

1.5 Thesis layout 4

2 LITERATURE REVIEW **5**

2.1 Historical background of TEG 5

2.2 Thermoelectric power generators basic configuration 6

2.3 Categories of thermoelectric power generation 7

2.3.1 Low power generation 7

2.3.2 High power generation 8

2.4 Performance of TEG 9

2.5 Seebeck Effect 11

2.6 Factors affecting TEG performance 12

2.6.1 The influence of temperature gradient 13

2.6.2 The impact of heat source temperature 13

2.6.3 The impact of load resistance 13
2.6.4 The impact of phonon thermal conductivity of TEM 14
2.7 Thermoelectric figure of merit 16
2.8 Categories of TEM 17
2.9 Thermoelectric material: Penta-Graphene 19
2.10 Molecular dynamics simulation 20
2.10.1 The Verlet algorithm 22
2.10.2 Interatomic potential 23
2.11 Boltzmann transport theory 24
2.11.1 The diffusion induced evolution of $f_k(r)$ 25
2.11.2 The external field induced evolution of $f_k(r)$ 26
2.11.3 The scattering induced evolution of $f_k(r)$ 26

3 METHODOLOGY **30**
3.1 Overview of the research methodology 30
3.2 Non equilibrium molecular dynamics simulation 30
3.3 Boltzmann transport equation 32
3.4 Software requirement 33

4 RESULTS AND DISCUSSIONS **34**
4.1 Overview 34
4.2 Phonon thermal conductivity 34
4.3 Electronic thermal conductivity 36
4.4 Electric conductivity 36
4.5 Seebeck coefficient 37
4.6 Power factor 38
4.7 Total thermal conductivity 40
4.8 Thermoelectric figure of merit 41
4.9 Efficiency of PG based TEG 42

5 CONCLUSIONS AND RECOMMENDATIONS **44**
5.1 Conclusions 44
5.2 Recommendations 44
Appendices 51

List of Tables

3.1 Specification of temperatures used to investigate phonon thermal conductivity of PG 31
3.2 Electron relaxation time of PG at different temperature 32

List of Figures

2.1 Thermoelectric power generator 7
2.2 Scheme of the TEG 10
2.3 Maximum conversion efficiency (η_{max}) as a function of temperature difference (ΔT) over the mid-temperature range for different TEM based TEG . . 11
2.4 Seebeck effect: Electric potential formation in response to the temperature gradient applied along the open-circuit channel. 12
2.5 ZT values for state-of-the-art TEMs in the last 3 years 17
2.6 Structure of PG 20
2.7 Molecular dynamics basic algorithm 21
2.8 At time $t = 0$ particles at position $r - \delta t v_k$ reach the position r at a later time δt 25

3.1 Methodology flowchart 30
3.2 The three stages of performing NEMD simulation of heat transport at temperature 150K 31

4.1 K_p of PG as a function of temperature 35
4.2 Electronic thermal conductivity of PG as function of temperature 36
4.3 Electric conductivity of PG as function of temperature 37
4.4 Seebeck coefficient of PG as function of temperature. 38
4.5 Power factor of PG as a function of temperature 39
4.6 Total thermal conductivity of PG as a function of temperature 40
4.7 ZT of PG as a function of temperature. 41
4.8 Performance of PG-based TEG 42

List of acronyms and abbreviations

TEG	Thermoelectric Generator
TEM	Thermoelectric Material
LAMMPS	Large-scale Atomic/Molecular Massively Parallel Simulator
MD	Molecular Dynamics
NEMD	Non-Equilibrium Molecular Dynamics
PG	Penta-Graphene
I	Current
V	Voltage
R_L	Load Resistance
STEG	Solar Thermoelectric Generator
RTG	Radioisotope Thermoelectric Generator
IoT	Internet of Things
GPHS	General Purpose Heat Source
ZT	Thermoelectric Figure of Merit
P	Output Electric Energy
Q	Provided Thermal Energy
Tlo	Lower Temperature
Thi	Higher Temperature
BST	Bismuth Tellurium Selenide
TAGS	Tellurium Silver Germanium Antimony
T_h	Hot side Temperature
T_c	Cold side Temperature
K_e	Electronic Thermal conductivity
K_p	Phononic Thermal conductivity

Abstract

A thermoelectric generator (TEG) is a device that generates electricity by utilizing the Seebeck effect, which creates an electric potential difference in response to a temperature difference. The TEG relies on thermoelectric materials (TEMs) to convert heat into electricity. Researchers are looking for TEMs with low thermal conductivity and penta-graphene (PG) has displayed promising properties when compared to graphene. The performance of a PG-based TEG is assessed through simulations that take into account temperature gradients and the thermoelectric figure of merit (ZT) parameter, which is a measure of the TEG's performance that combines the Seebeck coefficient, electrical conductivity and thermal conductivity. The study employs non equilibrium molecular dynamics (NEMD) calculate the phononic thermal conductivity (K_p) and the Boltztrap code to calculate the electronic thermal conductivity (K_e), electric conductivity and seebeck coefficient of PG. The findings indicate that PG exhibits a lower phononic thermal conductivity compared to graphene. At a temperature of 300 K, PG demonstrated a ZT value of 0.15, which is 16.6 times higher than the ZT value of 0.009 observed for graphene. Furthermore, the ZT value of PG increases with rising temperature, reaching 0.52 at 900K. To assess the efficiency of the PG-based TEG, the hot side temperature was varied while maintaining the cold side at 300K. As a result, an efficiency of 7% was achieved when the hot side temperature reached 900K. These findings suggest that PG is a suitable TEM and has the potential to enhance the performance of TEGs. Future research can further explore the use of PG as a TEM and contribute to the development of efficient energy conversion in TEGs.

Keywords: Thermoelectric Generator, Seebeck Effect, Performance, Thermoelectric Figure of Merit

1. INTRODUCTION

1.1. Background of the study

A thermoelectric generator also known as a Seebeck generator, is a device that converts heat into electricity. It operates based on the Seebeck effect, which states that a temperature difference can create an electric potential difference. The core building block of a TEG is the TEM, which converts heat into electricity through the Seebeck effect (Radouane, 2023). Figure 2.1 shows the fundamental configuration of a TEG. The temperature difference across the TEM results in the production of direct current (DC) that flows towards a load (R_L). The load is defined by a terminal voltage (V) and a terminal current (I) and the electrical power generated can be calculated as I^2R_L or VI (Mary-Rose & WallenfeldtAn, 2024).

The performance of a TEG relies on two key factors: the temperature gradient (ΔT) and the ZT of the TEMs used. The energy conversion efficiency of TEG is defined as the output electric energy (P) divided by the provided thermal energy (Q) (Sun et al., 2022).

$$\eta = \frac{P}{Q} = \frac{\Delta T}{T_h} \frac{\sqrt{1+(ZT)_{avg}}-1}{\sqrt{1+(ZT)_{avg}}+\frac{T_c}{T_h}} \tag{1.1}$$

Where T_h is heat source temperature, T_c is heat sink temperature, ΔT is temperature difference and $(ZT)_{avg}$ is the average value of ZT of TEM.

To be considered suitable for use in TEGs, a TEM must possess a remarkably high Seebeck coefficient, which enables the production of a larger thermoelectric voltage and enhances the efficiency of power generation from heat. Additionally, a high level of electrical conductivity reduces resistive losses and improves the flow of electrical current, resulting in improved conversion efficiency. Finally, a low thermal conductivity helps minimize heat dissipation, allowing for better heat preservation and increased conversion of heat into electricity. These characteristics are crucial for enhancing the performance of a TEG (Snyder & Snyder, 2017).

In the search for TEMs that have low thermal conductivity, a two-dimensional PG has shown intriguing properties compared to graphene. Chen et al. (2017) investigated PG as

a TEM and found that at 700K temperature ZT value of PG is 0.14, which is higher than that of graphene (Deb et al., 2022). Furthermore, Wang et al. (2016) observed that the thermal conductivity of PG at room temperature is 645 W/(m·K), significantly lower than that of graphene (4000 W/(m·K)). Additionally, Muna & Winczewski (2020) reported a thermal conductivity of approximately 18.7 W/(m·K) for PG at a room temperature of 300 K. They also observed a decreasing trend in the thermal conductivity of PG with increasing temperatures.

The low thermal conductivity and high Seebeck coefficient of PG contribute to maximizing the efficiency of the TEG by reducing heat losses and maintaining a significant temperature gradient. The low thermal conductivity helps minimize heat conduction and prevent excessive thermal transfer. In this research work, we aim to analyze the performance of PG based TEG.

1.2. Statement of the problem

The ZT parameter, which comprises the Seebeck coefficient, electrical conductivity and thermal conductivity, is a critical factor when selecting suitable TEMs and optimizing the performance of TEGs. It is essential to identify materials with high Seebeck coefficients, high electrical conductivity and low thermal conductivity to enhance TEG performance. Moreover, factors such as cost-effectiveness, abundance on Earth and flexibility should also be considered. Consequently, further research is necessary to comprehend the performance of PG an organic TEM in TEGs.

Prior research has investigated the thermoelectric properties of PG. These studies have yielded intriguing results, revealing a noteworthy ZT value of 0.14 at 700K, which surpasses that of graphene. Furthermore, PG exhibits low thermal conductivity of 18.7 W/(m·K) at room temperature, indicating its potential as an organic TEM for the development of flexible and wearable self-powered TEGs. Despite these benefits, the maximum ZT of 0.75 at 300K for organic TEMs is lower than that of widely utilized chalcogenides such as BST (Bismuth-Antimony or Selenium-Telluride) compounds and Tin Selinide, which exhibit high ZT values of 2.2 around 773 K. These findings suggest that PG possesses unique attributes that make it a promising candidate for TEM. However, further investigation is necessary to gain a deeper understanding of its performance in TEG, including its behavior at different temperatures and the relationship between thermal conductivity and temperature.

The remarkable characteristics of PG show great potential for various applications, including in TEG. However, the efficiency of PG-based TEG has yet to be determined. Furthermore, the thermoelectric properties of PG, such as the Seebeck coefficient, electronic thermal conductivity and electric conductivity, have not been reported across a broad range of temperatures. Therefore, it is necessary to conduct research to thoroughly investigate PG-based TEG at different temperature ranges. To explore this further, this research aims to conduct a simulation-based performance analysis of a PG based TEG. The study will utilize NEMD by LAMMPS and Boltztrap code to investigate the thermoelectric properties of PG and assess its suitability as a TEM.

1.3. Objectives

1.3.1 General objective

The general objective of this research work is to analyse the performance of PG Based TEG through a simulation study.

1.3.2 Specific objectives

The specific objectives of this research work are:

- To calculate thermal conductivity of PG and its the temperature dependence.
- To calculate the ZT of PG.
- To calculate the efficiency of PG based TEG.

1.4. Significance of the study

The study of PG as a TEM and its application in TEGs has significant implications for energy conversion and efficiency. TEGs offer a promising method to convert waste heat into electricity, thereby improving overall energy utilization and efficiency. By analyzing the performance of a PG-based TEG, this study aims to contribute to the development of efficient energy conversion technologies. The low thermal conductivity and high Seebeck coefficient of PG have the potential to minimize heat losses and maintain a significant temperature gradient, leading to improved TEG performance. This research can provide valuable insights

into harnessing waste heat and maximizing energy efficiency through the utilization of PG in TEGs.

Energy conservation is a critical aspect of addressing global energy challenges and reducing reliance on fossil fuels. The development of efficient TEMs and TEGs plays a crucial role in achieving energy conservation goals. By investigating the thermoelectric properties of PG and evaluating its suitability as a TEM, this study contributes to the optimization of TEGs. The understanding gained from this research can aid in the design and development of advanced TEG systems that optimize energy conversion and minimize energy losses. The utilization of PG in TEGs can contribute to sustainable energy solutions by efficiently converting waste heat into usable electrical energy.

The ZT is a key parameter in TEM that determines their efficiency in converting heat into electricity. By assessing the efficiency of PG-based TEGs, this study aims to explore the potential of PG as a TEM for pollution reduction. High ZT values indicate improved thermoelectric performance, as they indicate a higher conversion efficiency of heat into electricity. By identifying materials with high ZT values, such as PG, it becomes possible to develop TEG that can effectively harness waste heat and reduce pollution associated with traditional energy conversion methods. This study contributes to the exploration of sustainable and environmentally friendly energy conversion technologies by evaluating the ZT of PG and its potential in TEG applications.

1.5. Thesis layout

The thesis is organized in five chapters and each chapter will discuss on different issues related to the thesis. Chapter 1: Under this chapter we describe in detail the background of the study, statement of the problem, objective of the study and significance of the study. Chapter 2: This chapter focuses on the review from previous studies that was made helpful to gain knowledge and to understand where we are going to study. Chapter 3: This chapter gives the description about the methods and mechanisms used for our study. Chapter 4: This chapter presents the results and discussion of the study. Chapter 5: Finally, a conclusion of the results obtained in the work and a proposed recommendation of a future work is presented under this chapter.

2. LITERATURE REVIEW

This chapter provides a comprehensive overview of TEGs and their operation based on the Seebeck effect. It emphasizes the importance of TEMs in TEGs and discusses the fundamental configuration of a TEG, as well as the parameters that significantly affect its performance, including the temperature gradient and the ZT. The ZT parameter, which combines the Seebeck coefficient, electrical conductivity and thermal conductivity, plays a crucial role in the selection of suitable TEMs. Furthermore, this chapter introduces PG, a two-dimensional material with low thermal conductivity, as a potential TEM. It presents previous studies on PG's thermoelectric properties and its optimization for TEGs. The key topics covered in this chapter include TEG, the Seebeck effect, factors influencing TEG performance, ZT and the application of MD simulation and Boltzmann transport theory.

2.1. Historical background of TEG

Seebeck reported his discoveries to the Prussian Academy of Sciences in 1821, detailing experiments in which a compass needle was deflected when placed near a closed loop made of two dissimilar conductors, one of which was heated. Although he mistakenly believed the interaction was magnetic in nature, he investigated the phenomenon across a wide range of materials, including some now known as semiconductors and arranged them in order of magnitude based on the product of Seebeck coefficient and electrical conductivity. The resulting "Seebeck series" is strikingly similar to the modern-day thermoelectric series. If Seebeck had used the first and last members of his series in a thermocouple, he could have converted thermal energy into electricity with an efficiency of approximately 3% in the 1820s, which is comparable to the most efficient steam engine of the time. In hindsight, Seebeck's account makes it clear that the observed phenomenon was caused by an electric current flowing in the circuit and he had discovered the first of the so-called Seebeck effect (Rowe, 1978). In 1885, Lord Rayleigh initially calculated the efficiency of a thermoelectric generator, but his calculation was incorrect. Later, in 1909 and 1911, Altenkirch provided a satisfactory theory of thermoelectric generation and established that good thermoelectric materials should possess high Seebeck coefficients and low thermal conductivity to retain

heat at the junction and low electrical resistance to minimize Joule heating (Rowe, 1978).

The combustion of fossil fuels for electricity and heat generation has resulted in increased greenhouse gas emissions, leading to the development of environmentally friendly and efficient alternative energy generation systems. One such system is the conversion of waste heat into electrical power. The development of various power generation systems, such as solar panels, wind turbines and geothermal power plants, aims to reduce reliance on fossil fuels and decrease greenhouse gas emissions. However, these systems often require expensive maintenance. In contrast TEGs provide a cost-effective solution to convert heat into electricity. TEGs can be used with heat sources of varying sizes and are highly reliable. Additionally, TEGs have a long lifespan and can effectively use low-grade thermal energy to generate electrical power. TEGs function based on the Seebeck effect, which converts thermal energy, specifically temperature differences into electrical energy (Mamur & Ahıska, 2014).

2.2. Thermoelectric power generators basic configuration

A thermoelectric power generator is a solid-state device that converts heat energy into electrical energy by utilizing the thermoelectric effect, specifically the Seebeck effect. This process occurs when there is an interaction between the flow of heat and electricity through solid materials (Mary-Rose & WallenfeldtAn, 2024). The basic configuration of a thermoelectric power generator follows a standardized structure, as shown in Figure 2.1 (Mary-Rose & WallenfeldtAn, 2024). The system consists of a heat source, a TEM, a heat transfer interface, a heat sink and a load.

The heat source acts as the provider of high temperature and the generated heat is transferred through the TEM towards the heat sink. The TEM plays a crucial role in converting heat energy into electrical energy through the Seebeck effect. The heat transfer interface serves as a connection between the heat source and the TEM, as well as between the TEM and the heat sink. It facilitates efficient thermal energy transfer and should possess electrical insulation properties. The heat sink is maintained at a lower temperature compared to the heat source, creating a temperature gradient across the TEM (Champier, 2017).

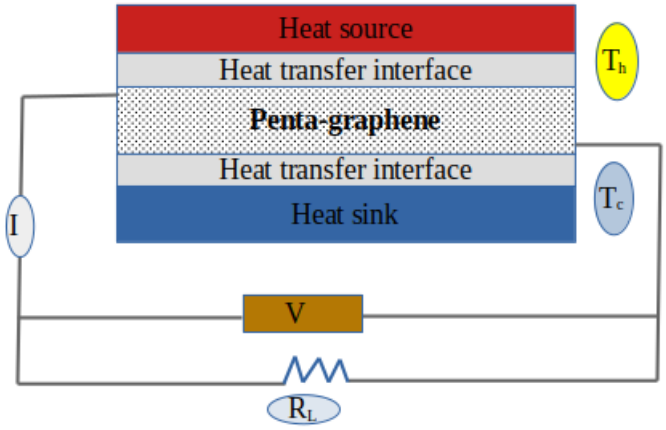

Figure 2.1: Thermoelectric power generator (Mary-Rose & WallenfeldtAn, 2024)

.

The heat sink is maintained at a lower temperature compared to the heat source, creating a temperature gradient across the TEM. This temperature difference leads to the generation of direct current that flows towards a load resistance. The load is characterized by a terminal voltage and a terminal current. The amount of electrical power generated is determined by the product of the square of the current and the load resistance, or simply the product of the voltage and the current.

2.3. Categories of thermoelectric power generation

Thermoelectric power generation is typically classified into two primary categories based on the amount of electrical power that can be generated: low power generation and high power generation.

2.3.1 Low power generation

Body-mounted electronic devices, such as smartphones, audio players and iPods, as well as medical devices like hearing aids and cardiac pacemakers, can be broadly categorized. These devices require energy sources that are both autonomous and competitive with batteries, which currently dominate the market for body-mounted devices that require between 5 μW and 1W of power and have a lifespan of 5 years or more. For instance, companies like Citizen and Seiko are now producing wristwatches with TEGs, with Seiko's watch having an efficiency of about 0.1% and an open-circuit voltage of 300mV at a temperature gradient

of 1.5K (Elsheikh et al., 2014).

2.3.2 High power generation

i) Waste heat TEG: TEGs offer a clever solution for reducing the negative consequences of global warming by converting waste heat into electrical energy, such as the heat generated by industrial processes like the steel industry and automobile engines. The steel industry and the automotive sector, which recognize the potential of waste heat as a valuable energy source, have played a significant role in the commercial development of TEGs for high-power electricity generation (Elsheikh et al., 2014).

Several automobile manufacturers such as Volvo, Volkswagen, Bayerische Motoren Werke (BMW) and Ford are working on creating TEG systems with power outputs of roughly 1 kilowatt. By employing a TEG with a ZT of 1.25 and an efficiency of around 10%, it is possible to recover 35-40% of the power from the exhaust manifold at an average temperature of 250°C. This recovered power could contribute to a significant improvement in efficiency, potentially increasing efficiency by up to 16% thermoelectric power generation (LeBlanc, 2014).

ii) Solar TEGs (STEGs): STEGs were originally intended for use in space applications due to their dependability, extended lifetimes and capacity to capture substantial levels of solar radiation in extraterrestrial locations. However, recent interest in these systems has shifted towards residential solar-thermal-energy harvesting. A STEG comprises a TEG and a thermal collector. The thermal collector absorbs solar heat, which is then concentrated and conducted to the generator through a fluid pipe or other means. The thermal resistance of the generator produces a temperature difference proportional to the heat flux, ultimately resulting in the generation of electricity (Elsheikh et al., 2014).

iii) Radioisotope thermoelectric generators (RTGs): Since 1961, the United States has utilized radioisotope RTGs to provide spacecraft with electrical power. To achieve the required power output, the selection of the appropriate number of general-purpose heat-source (GPHS) modules is crucial. Each GPHS module consists of a composite carbon body housing four fuel pellets and serving as an aero-impact shell. Plutonium dioxide ($^{238}PuO_2$) is used as the isotope fuel, with an approximate density of 80%. For power conversion, thermoelectric junctions like silicon-germanium (SiGe) junctions are employed (Elsheikh et al., 2014). The heat generated by the radioactive decay of ^{238}Pu in the fuel pellets, encapsulated

within the GPHS modules, is partially converted into electrical energy by the SiGe unicouples. Lead telluride was previously used as the TEM for lower-powered RTGs, operating at a maximum hot junction temperature of less than 865 K. However, SiGe thermoelectric elements were later adopted for high-powered RTGs due to the detrimental effects of oxygen on the RTG materials. Even at higher temperatures of up to 1275 K, sublimation rates and oxidation effects of these elements can be controlled by implementing sublimation barriers and using an inert cover gas during ground operation (Champier, 2017).

2.4. Performance of TEG

The TEG properties are governed by the coupling of Ohm and Fourier laws. A TEG consists of two legs of TEM, which are connected electrically in series and thermally in parallel. By connecting multiple thermocouples electrically in series, the Seebeck voltages generated by each junction add up, resulting in a higher output voltage. This series connection allows for increased voltage generation, which is desirable for practical applications (Jaziri et al., 2020). On the other hand, the thermocouples are connected thermally in parallel. This means that the hot side of all the thermocouples is connected together and the cold side of all the thermocouples connected together. This arrangement ensures that the heat is effectively conducted through the system, maximizing the temperature difference across the junctions and optimizing the efficiency of the TEG.

Figure 2.2 (Juárez-Huerta et al., 2022) shows a model of TEG which operates between two thermal reservoirs (heat source and heat sink) with temperatures T_h and T_c $(T_h \geq T_c)$, having external thermal conductances K_h and K_c , R is the internal resistance of TEM with electric current I flowing through, α the Seebeck coefficient and K, the thermal conductance of two arms of the couple in parallel, associated with the heat leak.

The performance of TEG is determined by the ZT of the TEM used and one essential aspect to enhance energy conversion efficiency is to increase the Seebeck coefficient (α) while minimizing internal resistance (R) and reducing contributions to thermal conductivity (Juárez-Huerta et al., 2022).

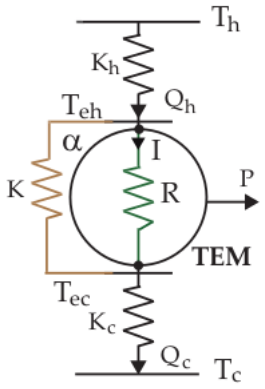

Figure 2.2: Scheme of the TEG (Juárez-Huerta et al., 2022).

The coupling between the gradients of temperature and electric potential shows the emergence of seebeck effect. The net rates of heat input and heat rejection at the TEM are given by

$$Q_h = IT_{eh}\alpha + K(T_{eh} - T_{ec}) - \frac{RI^2}{2} \tag{2.1}$$

$$Q_c = IT_{ec}\alpha + K(T_{eh} + T_{ec}) - \frac{RI^2}{2} \tag{2.2}$$

Where the first term corresponds to convective heat flow, with T_{eh} (T_{ec}) the effective temperature of TEM at hot (cold) side (Figure 2.2). The second represents heat leak between the cold and hot sides and the last term is the Joule heat received by each reservoir. For coupling with thermal sources, a Newtonian heat flow between a reservoir and TEM is assumed so that

$$Q_h = K_h(T_h - T_{eh}) \tag{2.3}$$

$$Q_c = K_c(T_{eh} - T_h) \tag{2.4}$$

The power output of the device is given by

$$P = Q_h - Q_c = I\alpha(T_{eh} - T_{ec}) - RI^2 \tag{2.5}$$

and the efficiency $\eta = \frac{P}{Q_h}$.

The maximum conversion efficiency (η_{max}) of TEGs varying with the temperature difference (ΔT) across the mid-temperature range is depicted in figure 2.3. As illustrated in the figure, different TEMs exhibit varying efficiencies at distinct temperature ranges (Hu et al., 2016).

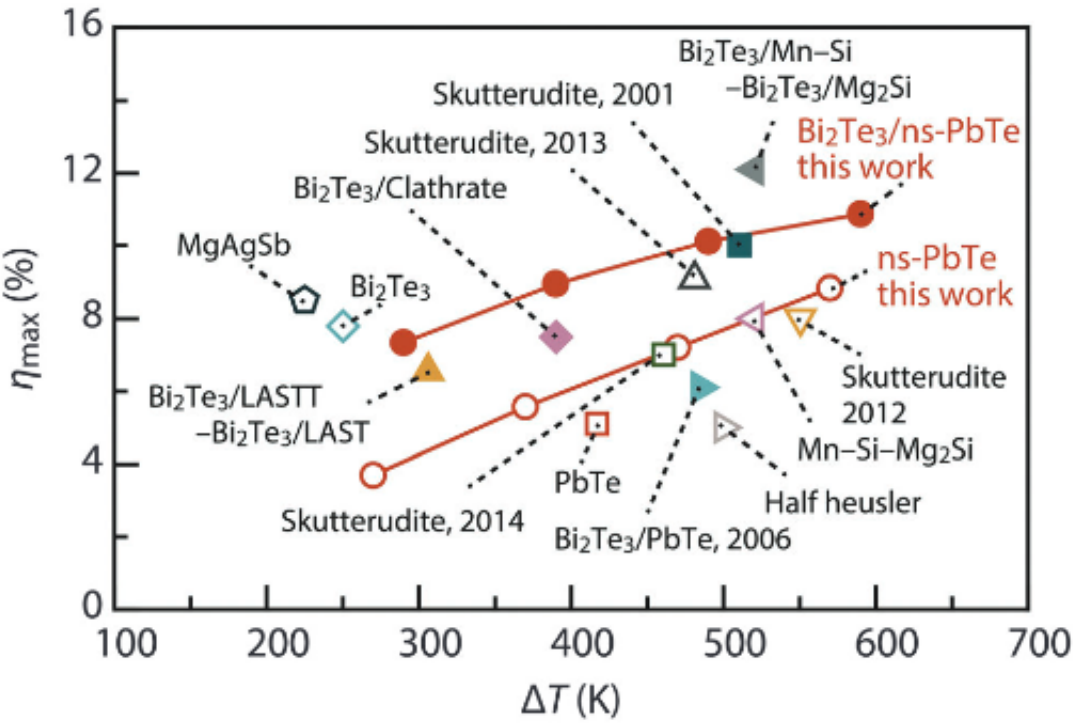

Figure 2.3: Maximum conversion efficiency (η_{max}) as a function of temperature difference (ΔT) over the mid-temperature range for different TEM based TEG (Hu et al., 2016).

2.5. Seebeck Effect

The Seebeck effect states that when two dissimilar metals are joined together and subjected to different temperatures (Li et al., 2019), a thermo-current and thermo-electromotive force exist in the joint circuit (He et al., 2015). This phenomenon occurs due to the movement of carriers, such as phonons and free electrons, which transport thermal energy from the hot end to the cold end of a material through diffusion mechanisms. As a result of this diffusion, an electric potential is also established across the material, as the population density of charge carriers increases at the cold end, sustained by the thermal energy diffusion. As shown in the figure 2.4 when a temperature gradient is applied along a conductive material, charge carriers move from the hot to the cold side and in the case of an open circuit, charge accumulation results in an electric potential difference. The Seebeck coefficient of a material represents the magnitude of the induced voltage in response to the temperature difference (Karamitaheri, 2013). The Seebeck voltage is the electromotive force that reacts to the buildup of charged carriers in the material and is mathematically defined as the product of the temperature gradient and the Seebeck coefficient (Dunham et al., 2019).

$$E_{emf} = -\alpha \nabla V \tag{2.6}$$

Where α seebeck coefficient, E_{emf} Electromotive force and ∇V voltage gradient. This term contributes to the electric current density, such that:

$$J = \sigma(-\nabla V + E_{emf}) \tag{2.7}$$

Where J current density and σ electrical conductivity. In the absence of electric current flow through the material, the Seebeck coefficient can be defined and measured, as the negative ratio of the local voltage and temperature gradients ∇T:

$$\alpha = -\frac{\nabla V}{\nabla T} \tag{2.8}$$

Equation 2.8 is valid for zero current flow through the material and for small temperature gradients, as the Seebeck coefficient is in general a temperature-dependent property.

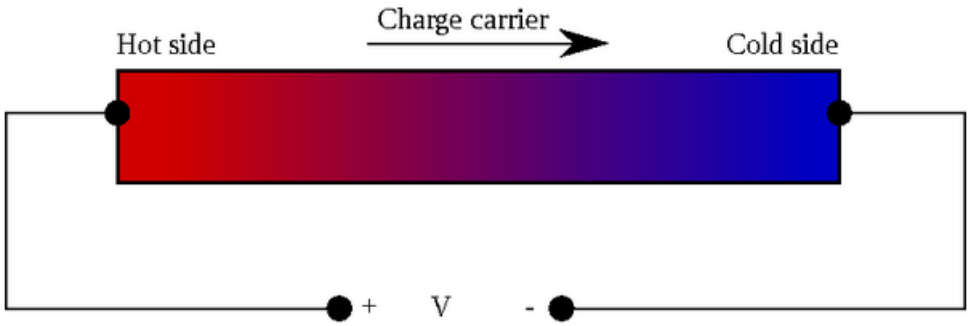

Figure 2.4: Seebeck effect: Electric potential formation in response to the temperature gradient applied along the open-circuit channel (Karamitaheri, 2013).

2.6. Factors affecting TEG performance

The performance of a TEG is influenced by several factors. These include the temperature difference across the TEG, the material properties of the TEMs used, the temperature of the heat source, the load resistance connected to the TEG, efficient heat dissipation, the geometry and configuration of the TEG modules and the environmental conditions. A larger temperature difference, favorable material properties (high Seebeck coefficient and electrical conductivity, low thermal conductivity), higher heat source temperatures, matching load

resistance, effective heat dissipation, optimized module design and suitable environmental conditions all contribute to improved TEG performance (B. S. B. Singh, 2023). Considering these factors the efficiency and power output of TEGs can be enhanced.

2.6.1 The influence of temperature gradient

The temperature gradient refers to the difference in temperature between the hot and cold sides of a TEG. The power output of the TEG is directly influenced by this temperature gradient. The TEG can produce a greater amount of electrical power by having a larger temperature difference, as it allows for a greater flow of heat. Consequently, when the temperature across the TEG increases, the maximum power output also increases. The Seebeck effect, which generates an electric potential when there is a temperature gradient, is responsible for the operation of a TEG. A higher temperature gradient results in a higher voltage output (B. Singh et al., 2017). Therefore, a larger temperature difference enables the TEG to generate more electrical power by increasing the flow of heat (Tundee et al., 2014).

2.6.2 The impact of heat source temperature

The temperature of the heat source is a crucial factor that significantly affects the performance of a TEG. It directly impacts the power generation capability of the TEG by influencing the temperature gradient between its hot and cold sides. When the heat source temperature is raised, it results in a larger temperature difference and a higher power output due to an increased temperature gradient. Therefore, increasing the heat source temperature has the potential to enhance the power output of the TEG. The study shows that using a high input energy and a heat collector with high absorptivity and low emissivity can yield favorable results in terms of achieving a TEG with superior performance (Cai et al., 2011).

2.6.3 The impact of load resistance

Load resistance is the external electrical resistance connected to a circuit or device, such as a TEG. The power output and efficiency of a TEG system are significantly influenced by the load resistance. The voltage and current generated by the TEG are dependent on the load resistance. Ohm's law establishes a direct relationship between the voltage across the load resistance, the current flowing through it and the value of the load resistance itself.

By selecting different load resistance values, it is possible to adjust the voltage and current levels to meet the specific requirements of an application. The power output is inversely influenced by the combined effect of the internal resistance and the load resistance (Lesage & Pagé-Potvin, 2013).

2.6.4 The impact of phonon thermal conductivity of TEM

The phonon thermal conductivity of a TEM, often represented by K_p or K_l, plays a crucial role in the performance of a TEG. This property is responsible for the ability of a material to transmit heat through lattice vibrations. In a TEG, it determines the efficiency of heat transfer from the hot side to the cold side of the device. When a temperature difference is applied across the TEM, heat flows in the direction of the cold side. The efficiency of this heat transfer has a direct impact on the performance of the TEG in converting heat energy into electrical energy (Baranowski et al., 2013).

A low thermal conductivity in the TEMs used in the TEG is desirable. This is because a low thermal conductivity reduces heat losses during the heat transfer process. When the thermal conductivity is low, more heat remains in the region where the temperature difference exists, allowing for a larger temperature gradient across the TEG. On the other hand, a high thermal conductivity can result in significant heat dissipation and reduce the temperature difference across the TEG. This reduces the voltage output and power generation capabilities of the TEG (Beltrán-Pitarch et al., 2018). Therefore, selecting TEMs such as PG with low thermal conductivity is crucial for optimizing the performance of a TEG.

Thermal conductivity is characterized as the transfer of energy due to a variance in temperature. Heat moves from areas with higher temperature to areas with lower temperature (I.-S. Liu, 1990). Heat conduction in a medium is said to be one-dimensional when conduction is significant in one dimension only and negligible in the other two primary dimensions, two-dimensional when conduction in the third dimension is negligible and three-dimensional when conduction in all dimensions is significant. The rate of heat conduction in a specified direction is proportional to the temperature gradient, which is the rate of change in temperature with distance in that direction.

Fourier's Law states that the rate of heat transfer through a material is directly proportional to the temperature gradient across the material. The derivation of Fourier's Law was explained with the help of an experiment which explained the rate of heat transfer through

a plane layer is proportional to the temperaure gradient across the layer and transfer area (I.-S. Liu, 1990).

Rate of heat conduction $\propto \frac{(cross\ section\ area)(temperature\ difference)}{thickness}$

Let T_1 and T_2 be the temperature difference across a small distance Δx of cross section area A, K_p is the phonon thermal conductivity of the material. Therefore in one dimensional the following is the equation used

$$Q_{cond} = K_p A \frac{T_1 - T_2}{\Delta x} = -K_p A \frac{\delta T}{\delta x} \tag{2.9}$$

The two dimensional form of the Fourier's Law is given as

$$\vec{q} = -K_p A \left(\frac{\delta T}{\delta x} + \frac{\delta T}{\delta y} \right) \tag{2.10}$$

The three dimensional form of the Fourier's Law is given as

$$\vec{q} = -K_p A \left(\frac{\delta T}{\delta x} + \frac{\delta T}{\delta y} + \frac{\delta T}{\delta z} \right) = -K_p A \nabla T \tag{2.11}$$

In this research work the K_p of a two-dimensional PG determined by applying Fourier's Law which is utilized in NEMD.

$$J_x = -K_p \frac{\partial T}{\partial x} \tag{2.12}$$

$$K_p = -\frac{J_x}{\frac{\partial T}{\partial x}} \tag{2.13}$$

$$K_p = -\frac{\left(\frac{\triangle Q}{2S\triangle t} \right)}{\frac{\partial T}{\partial x}}. \tag{2.14}$$

For the calculation of heat flux J_x , we need to account for the amount of heat energy Q which flows per unit time t across the cross-sectional area S perpendicular to the transport direction (Muna & Winczewski, 2020). The area S is then computed from twice of height (since the energy flows in two directions) multiplied by thickness h of PG.

2.7. Thermoelectric figure of merit

The performance of a TEG is heavily influenced by the ZT of the material used in it. The ZT, which is a critical parameter, is used to evaluate the efficiency of the TEM (Snyder & Snyder, 2017). It measures how effectively the material can convert temperature differences into electrical voltage and consequently, power output. The ZT value is calculated using three key material properties: the Seebeck coefficient α, electrical conductivity σ, and thermal conductivity K, which are interrelated and determine the performance of the TEM.

The Seebeck coefficient, also known as the thermoelectric power or thermopower, measures the magnitude of the electric potential or voltage generated in a material when there is a temperature difference across it. It quantifies the ability of a material to convert a thermal gradient into an electrical voltage. The Seebeck coefficient expressed in units of microvolts per Kelvin ($\mu V/K$) or millivolts per Kelvin (mV/K). A higher Seebeck coefficient indicates a greater ability of the material to generate voltage in response to a temperature gradient. The electrical conductivity measures the material's ability to conduct electric charge. Electrical conductivity is typically expressed in units of Siemens per meter (S/m) or Siemens per centimeter (S/cm). A higher electrical conductivity implies that the material allows for better flow of electric current. The thermal conductivity measures the ability of a material to transfer thermal energy through conduction. Thermal conductivity is typically expressed in units of Watts per meter-Kelvin (W/m·K). A low thermal conductivity indicates that the material is a poor conductor of heat, while a high thermal conductivity suggests efficient heat conduction (Meng et al., 2015).

A higher ZT value suggests better thermoelectric performance (Snyder & Snyder, 2017). It indicates that the material exhibits a higher voltage output and enhanced efficiency in converting heat energy into electrical energy. A larger ZT value reflects a more favorable balance between the Seebeck coefficient, electrical conductivity and thermal conductivity of the material. The potential of a material for thermoelectric applications is determined in large part by a measure of the material's ZT written in Equation 2.15,

$$ZT = \frac{\alpha^2 \sigma T}{K} \tag{2.15}$$

where α is the Seebeck coefficient, σ the electrical conductivity and K is thermal conductivity the sum of two contributions : (i) electrons thermal conductivity (K_e) and (ii) phonons

thermal conductivity (K_p) and T is the absolute temperature of the material at the point in question (Eivari et al., 2021). Equation (2.15), shows that, to maximize the ZT of a material, it must meet the following criteria: (i) low thermal conductivity to maintain a considerable temperature difference between the two ends of the material; (ii) high electrical conductivity to reduce the internal resistance of the material; and (iii) a high Seebeck coefficient (Zide et al., 2006), required to obtain a high voltage. Frequently, the interdependence of these factors presents challenges in attaining a TEM with a high ZT value (Snyder & Toberer, 2008).

Numerous noteworthy research studies have demonstrated that scientists worldwide are consistently striving to enhance the practicality of commercial-scale TEG (Ramasubramanian et al., 2022). However, the pursuit of this goal is confronted with several difficulties due to the inadequate efficiency of TEMs. The last 3 years of state-of-the-art, best performing TE materials ZT are summarized in figure 2.5 (d'Angelo et al., 2023).

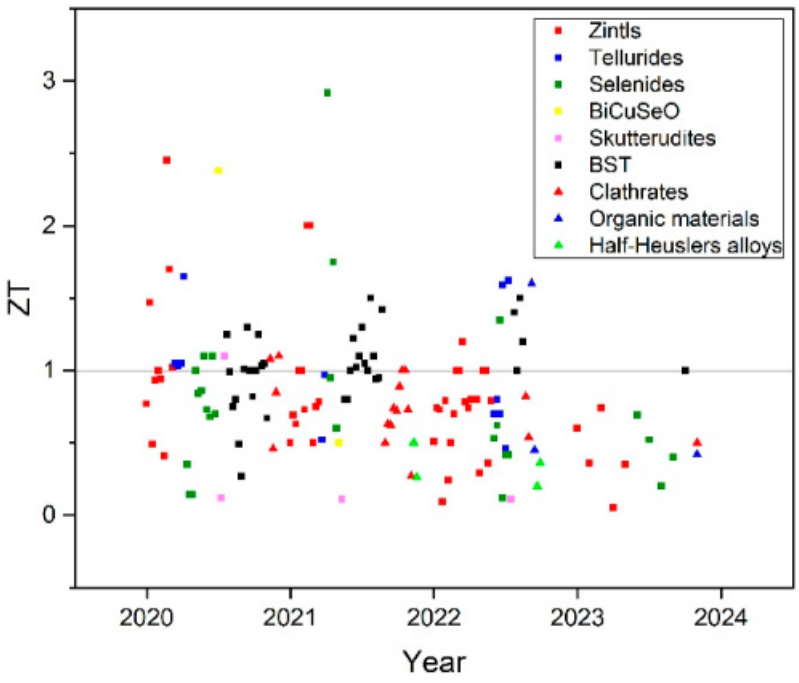

Figure 2.5: ZT values for state-of-the-art TEMs in the last 3 years (d'Angelo et al., 2023).

2.8. Categories of TEM

TEMs can be classified based on various factors such as chemical composition, application and temperature range (d'Angelo et al., 2023). The classification primarily depends on the material composition, with secondary consideration given to the application and temperature. State-of-the-art TEMs can be grouped into eight main categories: skutterudites

(SKUs), half-Heusler, clathrates, zintls, oxyselenides, silicon-germanium alloys (Si-Ge), chalcogenides, and organic and hybrid materials. Additionally, these materials are further categorized based on their temperature ranges.

In the low-temperature range (up to 600 K), TEMs find applications in wearable and medical devices operating near room temperature. It also includes microelectronics applications, such as nodes for wireless sensor network (WSN) devices, due to their low heat generation.

The medium-temperature range (from 600 to 1000 K) is commonly targeted for thermoelectric applications in the automotive industry and industrial settings. Waste heat can be efficiently converted into electrical current directly from the engine in automotive applications, while industrial plants, such as heat pipes, can also benefit from thermoelectric energy conversion in this temperature range.

In the high-temperature range (above 1000 K), TEMs are predominantly employed in aerospace applications to harvest energy for space missions and outer space exploration. This range becomes crucial in situations where traditional photovoltaic energy harvesting methods are not feasible.

Carbon-based materials including PG are organic TEMs that hold significant potential for the development of flexible and wearable self-powered devices, which are currently lacking in the market but extensively researched. These organic materials offer several advantages over traditional chalcogenides like bismuth telluride, such as lower cost, greater availability on Earth and intrinsic flexibility. Additionally, they exhibit high thermoelectric performance around room temperature, making them particularly suitable for addressing the increasing demand for wearable and flexible devices driven by the rapid growth of the Internet of Things (IoT). Researchers have been investigating the implementation of TEMs in polymers and other organic materials as a potential solution. However, achieving high thermoelectric efficiency remains a challenge, with highly performing polymeric materials reaching ZT values no higher than 0.75 (Fan et al., 2018). This limitation is primarily attributed to the extremely low electrical conductivity and Seebeck coefficient exhibited by these materials. While they are currently employed as substrates or supports for chalcogenides operating at low temperatures (e.g., Bi_2Te_3) (Jaziri et al., 2020), the integration of TEMs into polymers and organic materials is an ongoing research area.

2.9. Thermoelectric material: Penta-Graphene

Zhang et al. (2015) proposed a TEM called pentagonal graphene that distinguishes itself from typical carbon structures composed of hexagonal building blocks (Zhang et al., 2015). PG is exclusively made up of carbon pentagons and offers several advantageous characteristics. Firstly, it exhibits high carrier mobility, enabling efficient electrical conduction. Additionally, PG demonstrates significantly lower thermal conductivity compared to graphene (Gu & Yang, 2016) (Abbood & Jabour, 2017) , indicating its potential for efficient conversion of heat into electricity. With an expected capability to withstand temperatures up to 1000 K, PG possesses extraordinary features such as a rare negative Poisson's ratio and exceptionally high ideal strength, surpassing that of graphene. These remarkable properties position PG as a highly promising material for a range of applications, including TEG (Xu et al., 2015).

The crystal structure of PG has a tetragonal structure with the optimized lattice constant $a = b = 3.64$. Each unit cell has a layered structure containing six atoms (two sp^3 and four sp^2 hybridizied carbon atoms denoted as C1 and C2). In contrast to the perfectly planar graphene, it can be seen from the side view of PG that there is an interlayer buckling where C1 atoms are situated in the middle layer with $z = 0$ whilst C2 atoms are in the upper and lower layers with $z = \pm h$. Here, h denotes the interlayer spacing which equals 0.6 Å, leading to a two dimensional sheet with a total thickness of 1.2 Å. In PG the carbon-carbon bonds have the lengths $d1 = 1.55$ (all C1-C2 bonds) and $d2 = 1.34$ (all C2-C2 bonds).

The interior bond angles of pentagons are equal to 113.5 (C1-C2-C2 angle, occurs twice), 112.4 (C1-C2-C1 angle) and $\alpha = 98.6$ degrees (C2-C1-C2 angle, also occurs twice) (Muna & Winczewski, 2020). There is also another C2-C1-C2 angle, which measures the wrinkles of the PG structure. According to Zhang it is equal to $\beta = 134.4$ degrees, indicating the distorted sp^3 nature of C1 atoms. One unit cell of PG contains 3 atom types as shown in the figure 2.6 (red, blue and yellow color) with 2 atoms for each type (Muna & Winczewski, 2020).

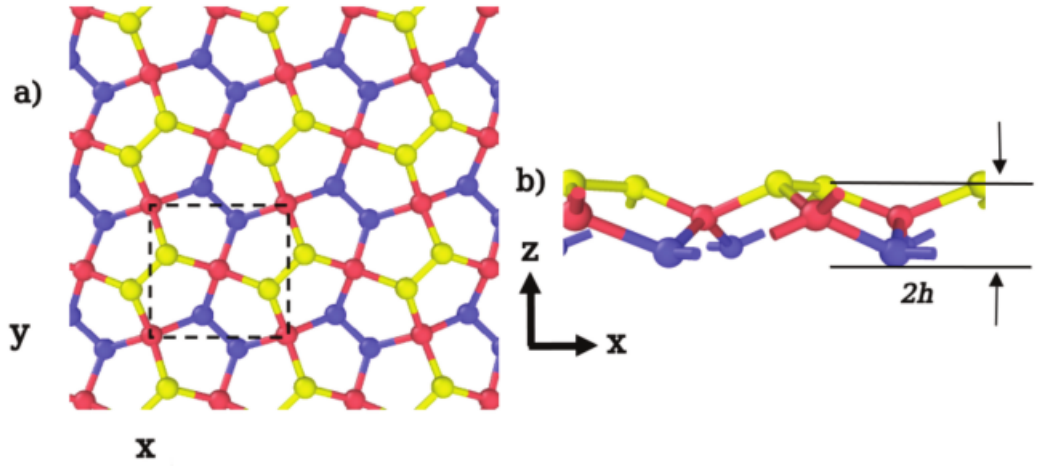

Figure 2.6: Structure of PG (Muna & Winczewski, 2020).

2.10. Molecular dynamics simulation

Computer simulations play a crucial role in studying molecular assemblies, providing insights into their structure and microscopic interactions that complement traditional experiments (Dror et al., 2012). Simulations serve as a bridge between theory and experiment, allowing testing of theories by comparing simulated models with experimental data. Conversely, simulations can validate or refine models by comparing them against experimental observations. Simulations also enable the exploration of extreme conditions that may be challenging or impossible to achieve in the laboratory, such as high or low temperatures and pressures (Allen & P, 2004).

MD energy calculations involve the determination of the potential and kinetic energies in a molecular system, while forces are obtained by differentiating the potential energy with respect to atomic positions. Numerical integration methods are then employed to update the positions and velocities of the atoms, allowing the simulation to progress in time.

$$F_i = m_i a_i = m_i \frac{dv_i}{dt} = m_i \frac{d^2 x_i}{dt^2} = -\frac{\partial E_{pot}}{\partial x_i} \tag{2.16}$$

Where F_i is forces component, E_{pot} potential energy, v_i velocity of particles, m_i mass of particles and x_i atom coordinates. These calculations and techniques form the foundation of MD simulations, which are powerful tools for investigating the behavior of atoms and molecules at the molecular level. MD integrates Newton's equations of motion to simulate interactions between particles representing atoms, molecules, electrons, clusters or larger clumps focus-

ing on short-range interaction models, utilizing neighbor lists for efficient handling of large systems (Allen & P, 2004).

Many different methods can be used to integrate the Newton's equations of motion. The Velocity Verlet algorithm is one of the integration schemes available in LAMMPS for advancing the equations of motion in time. Once the system is built, forces acting on every atom are obtained by deriving equations, the force-fields, where potential energy is deduced from the molecular structure. Force-fields are complex equations, but they are easy to calculate as shown in figure 2.7 (Hospital et al., 2015).

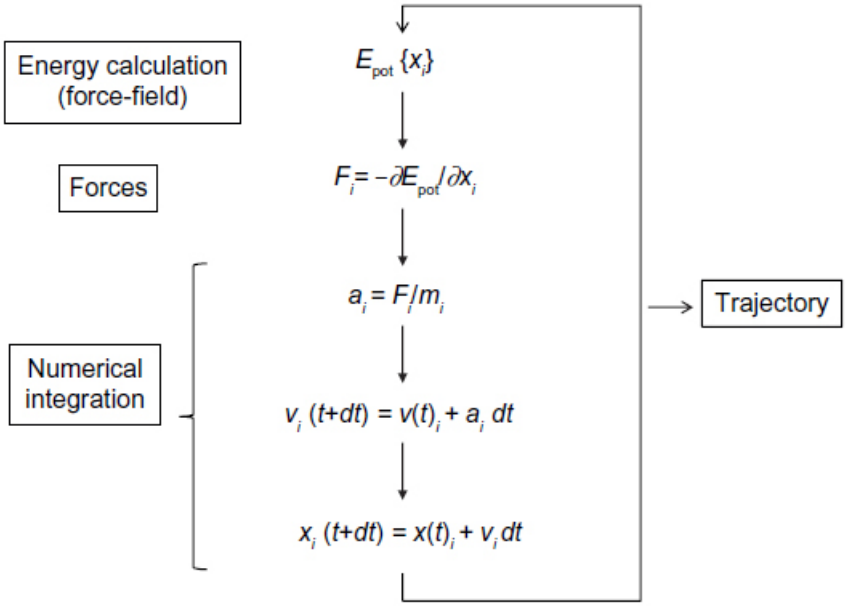

Figure 2.7: Molecular dynamics basic algorithm (Hospital et al., 2015).

Where E_{pot} potential energy, t simulation time and dt iteration time. For each spatial coordinate of the N simulated atoms i, x atom coordinate, F forces component, a acceleration, m atom mass and v velocity.

The approach we employ to calculate the phonon component of thermal conductivity, known as NEMD or the direct method, involves the creation of a heat source and a heat sink within the system. By closely monitoring the heat flow and temperature gradients, we can determine the thermal conductivity. In NEMD, we impose a temperature gradient on the system and measure the resulting heat flux. The thermal conductivity can then be determined using the principles of Fourier's law.

2.10.1 The Verlet algorithm

The Velocity Verlet algorithm is a numerical integration method commonly used in MD simulations. It updates the positions and velocities of particles based on the forces acting on them (Ercolessi, 1997). The basic idea is to write two third-order Taylor expansions for the positions $r(t)$, one forward and one backward in time, v the velocities, a the accelerations and b the third derivatives of r with respect to t;

$$r(t+\Delta t) = r(t) + v(t)\Delta t + \frac{1}{2}a(t)\Delta t^2 + \frac{1}{6}b(t)\Delta t^3 + O(\Delta t^4) \tag{2.17}$$

$$r(t-\Delta t) = r(t) - v(t)\Delta t + \frac{1}{2}a(t)\Delta t^2 - \frac{1}{6}b(t)\Delta t^3 + O(\Delta t^4) \tag{2.18}$$

Adding the two expressions gives

$$r(t+\Delta t) = 2r(t) - r(t-\Delta t) + a(t)\Delta t^2 + O(\Delta t^4) \tag{2.19}$$

This is the basic form of the Verlet algorithm. Newton's equations, $a(t)$ is just the force divided by the mass and the force is in turn a function of the positions $r(t)$:

$$a(t) = -\frac{1}{m}\nabla V(r(t)) \tag{2.20}$$

where ∇V is potential gradient.

The truncation error of the algorithm when evolving the system by Δt is of the order of Δt^4, even if third derivatives do not appear explicitly. This algorithm is at the same time simple to implement, accurate and stable explaining its large popularity among MD simulators (Ercolessi, 1997). A problem with this version of the Verlet algorithm is that velocities are not directly generated. While they are not needed for the time evolution, their knowledge is sometimes necessary. Moreover, they are required to compute the kinetic energy K, whose evaluation is necessary to test the conservation of the total energy $E = K + V$. This is one of the most important tests to verify that a MD simulation is proceeding correctly. One could compute the velocities from the positions by using

$$v(t) = \frac{r(t+\Delta t) - r(t-\Delta t)}{2\Delta t} \tag{2.21}$$

However the error associated to this expression is of order Δt^2 rather than Δt^4. To overcome this difficulty, some variants of the Verlet algorithm have been developed. They give rise to exactly the same trajectory and differ in what variables are stored in memory and at what times. The better implementation of the same basic algorithm is the so-called velocity Verlet scheme, where positions, velocities and accelerations at time $t+\Delta t$ are obtained from the same quantities at time t in the following way:

$$r(t+\Delta t) = r(t) + v(t)\Delta t + \frac{1}{2}a(t)\Delta t^2 \tag{2.22}$$

$$v(t+\frac{\Delta t}{2}) = v(t) + \frac{1}{2}a(t)\Delta t \tag{2.23}$$

$$a(t+\Delta t) = -\frac{1}{m}\nabla V(r(t+\Delta t)) \tag{2.24}$$

$$v(t+\Delta t) = v(t+\frac{\Delta t}{2}) + \frac{1}{2}a(t+\Delta t)\Delta t \tag{2.25}$$

2.10.2 Interatomic potential

Interatomic potential is an important key to accurately examine results from MD simulations. There is a variety of empirical potentials to describe the interactions between carbon atoms and the commonly used ones are the Tersoff potentials, the second-generation reactive empirical bond order (REBO) potential and the environment-dependent interatomic potential (EDIP). In the previous research (De Sousa et al., 2021), it has been shown that there is only one potential which correctly describes all the important features of PG among empirical potentials available for the elemental carbon, namely a new parameterization of the Tersoff potential (Tersoff, 1989) proposed by Erhart and Albe in 2005 (Erhart & Albe, 2005).

The formula of the total potential energy U_{tot} of the system composed of N atoms within the Tersoff potential is given by:

$$U_{tot} = \sum_i \sum_{j>i} f_c r_{ij} \left[V_R(r_{ij}) - \frac{b_{ij}+b_{ji}}{2} V_A(r_{ij}) \right] = \sum_i \sum_{j>i} V_{ij} \tag{2.26}$$

Here, r_{ij} denotes the distance between atoms i and j. The functions $V_R(r_{ij})$ and $V_A(r_{ij})$ describe the repulsion and attraction and both have an exponential form. The factor $b_{ij} = \frac{b_{ij}+b_{ji}}{2}$ which occurs before the second term is the bond order. By scaling the attractive

term V_A it controls the bond strength, enabling a simultaneous description of single, double and triple covalent bonds. The b_{ij} parameter depends on the configuration of the system in the vicinity of atoms i and j. This causes the Tersoff potential to be a many-body potential (Tersoff, 1989). The cut-off function $f_c(r)$ smoothly turns off the interactions between distant atoms, causing that it is only the contributions of pairs of atoms which are covalent bonded that are included in the double summation (Muna & Winczewski, 2020).

2.11. Boltzmann transport theory

The Boltzmann transport theory is a vital tool for connecting microscopic and macroscopic quantities in electron transport studies. It enables us to understand electron behavior through quantities like diffusion coefficient and conductivity. The Boltzmann Transport Equation combines classical mechanics with quantum scattering rates to accurately describe electron gas transport properties, considering both the particle's motion and dissipate processes during energy state transitions. The electron distribution function plays a key role in electron transport analysis, providing insights into properties like electrical conductivity, electronic thermal conductivity and Seebeck coefficient. These properties are essential for evaluating TEM performance in TEG (J. Singh, 2008). Under equilibrium conditions, the electron distribution can be characterized by the Fermi-Dirac function,

$$f(E) = \frac{1}{exp(\frac{E-E_F}{K_B T}) + 1} \tag{2.27}$$

where k_B is the Boltzmann constant, T is the temperature, $f(E)$ the probability that a particle will have energy E and E_F is the fermi energy. The equilibrium electron gas is described by this distribution function. As long as external influences that could disrupt the equilibrium are absent, the Fermi-Dirac function will consistently determine the overall distribution of electrons, even when collisions continually transfer electrons from one k-state to another.

In order to describe the distribution function in the presence of external forces, notation $f_k(r)$ used to represent the local concentration of electrons in state k in the vicinity of r. The Boltzmann method involves analyzing how $f_k(r)$ changes over time. The variations in the electron distribution in k-space and r-space can be attributed to three distinct factors (J. Singh, 2008). Electron motion (diffusion) causes carriers to continuously enter and exit any given volume element around position r. External forces exerted on electrons cause them

to change their momentum (or wave vector) according to $\hbar dk/dt = F_{ext}$. Scattering processes cause electrons to transition from one k-state to another.

2.11.1 The diffusion induced evolution of $f_k(r)$

As shown in figure 2.8 if v_k represents the velocity of a carrier in state k, within a time interval t, the electron will travel a distance of $v_k t$. Consequently, the number of electrons in the vicinity of r after time δt will be equivalent to the number of carriers in the vicinity of $r - \delta t v_k$ at time 0.

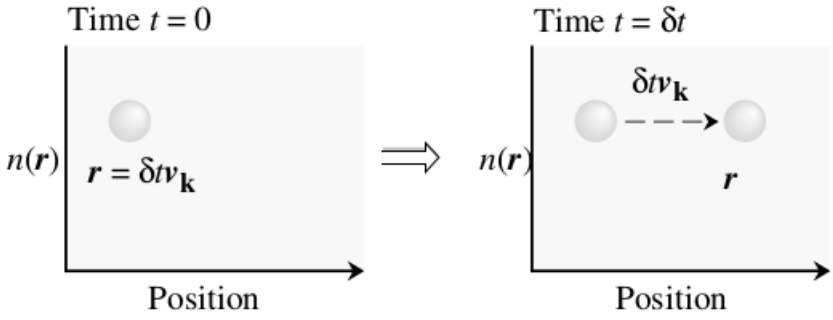

Figure 2.8: At time $t = 0$ particles at position $r - \delta t v_k$ reach the position r at a later time δt (J. Singh, 2008).

As a result of diffusion, we can establish the following equality (J. Singh, 2008),

$$f_k(r, \delta t) = f_k(r - \delta t v_k, 0) \tag{2.28}$$

By employing a Taylor series expansion, equation 2.28 can be expanded and expressed in the following manner.

$$f_k(r,0) + \frac{\partial f_k}{\partial t}.\delta t = f_k(r,0) - \frac{\partial f_k}{\partial r}.\delta t v_k \tag{2.29}$$

furthermore, the above equation is reduced to

$$\left.\frac{\partial f_k}{\partial t}\right|_{diff} = -\frac{\partial f_k}{\partial r}.v_k \tag{2.30}$$

2.11.2 The external field induced evolution of $f_k(r)$

The electron's crystal momentum k, changes in response to external forces according to Newton's equation of motion (J. Singh, 2008). The rate of change of k for an electric and magnetic field (E and B) is given by

$$\dot{k} = \frac{e}{\hbar}\left[E + v_k \times B\right] \tag{2.31}$$

The same as the diffusion-induced changes, we can propose that particles with momentum $k - \dot{k}\delta t$ at time $t = 0$ will possess momentum $\mathbf{k}$ at time δt, and

$$f_k(r, \delta t) = f_{k-\dot{k}}\delta t(r, 0) \tag{2.32}$$

By utilizing the Taylor series expansion on equation 2.32, we can express it in the following manner.

$$\left.\frac{\partial f_k}{\partial t}\right|_{ext.forces} = -\dot{k}\frac{\partial f_k}{\partial k}$$

$$= \frac{-e}{\hbar}\left[E + v_k \times B\right]\frac{\partial f_k}{\partial k} \tag{2.33}$$

Where e is electron charge and $\hbar$ Planck's constant.

2.11.3 The scattering induced evolution of $f_k(r)$

Assuming that the scattering processes are local and instantaneous, the change in an electron's state from k to k' can be described by the scattering rate function $W(k,k')$. This function represents the rate at which electrons scatter from state k to state k' when state k is occupied and state k' is empty. This scattering process leads to a change in the electron distribution function $f_k(r)$ over time (J. Singh, 2008).

$$\left.\frac{\partial f_k}{\partial t}\right|_{scattering} = \int \left[f_{k'}(1 - f_k)W(k',k) - f_k(1 - f_{k'})W(k,k')\right]\frac{d^3k'}{(2\pi)^3} \tag{2.34}$$

In equation 2.34 $(2\pi)^3$ in the denominator represents the number of allowed states within a k-space volume element d^3k'. The first term in the integral corresponds to the rate at which electrons transition from an occupied k' state (indicated by the factor $f_{k'}$) to an unoccupied k

state (indicated by the factor $(1-f_k)$). This term represents the gain of electrons. The second term represents the loss of electrons, as it corresponds to the rate at which electrons transition from an occupied k state (indicated by the factor f_k) to an unoccupied k' state (indicated by the factor $(1-f_{k'})$).

In a steady-state condition, the electron distribution function remains constant over time. This means that the sum of the gain and loss terms in the expression for the rate of change of the distribution function will be zero, indicating that there is no net change in the distribution function. In other words, the partial derivative terms calculated earlier will cancel out, resulting in a zero net change in the distribution function under steady-state conditions.

$$\left.\frac{\partial f_k}{\partial t}\right|_{scattering} + \left.\frac{\partial f_k}{\partial t}\right|_{diff} + \left.\frac{\partial f_k}{\partial t}\right|_{ext.forces} = 0 \tag{2.35}$$

Let us introduce the following:

$$g_k = f_k - f_k^0 \tag{2.36}$$

where f_k^0 is the equilibrium distribution. Now let us compute g_k, which quantifies the deviation of the distribution function from the equilibrium state. Substituting the partial time derivatives resulting from diffusion and external fields into the expression for the rate of change of the electron distribution function the resulting expression is given by:

$$-v_k.\nabla_r f_k - \frac{e}{\hbar}\left[E + v_k \times B\right].\nabla_k f_k = -\left.\frac{\partial f_k}{\partial t}\right|_{scattering} \tag{2.37}$$

Replacing $f_k = g_k + f_k^0$

$$\begin{aligned} &-v_k.\nabla_r f_k^0 - \tfrac{-e}{\hbar}\left[E + v_k \times B\right].\nabla_k f_k^0 \\ &= -\left.\frac{\partial f_k}{\partial t}\right|_{scattering} + v_k.\nabla_r g_k + \frac{e}{\hbar}[E + v_k \times B].\nabla_k g_k \end{aligned} \tag{2.38}$$

The magnetic force term on the left-hand side of Equation 2.38 is directly proportional to the expression $v_k \frac{e}{\hbar}(v_k \times B)$. Since this expression evaluates to zero, the magnetic force term itself is also zero. Let us recall

$$v_k = \frac{1}{\hbar}\frac{\partial E_k}{\partial k} \tag{2.39}$$

The variable E_k represents the energy of the particle. We know that E_F, commonly denoted

as μ, at zero absolute temperature. Therefore, the equilibrium distribution function f_k^0 is given by the expression for the Fermi-Dirac distribution.

$$f_k^0 = \frac{1}{exp\left[\frac{E_k-\mu}{k_BT}\right]+1} \tag{2.40}$$

consequently

$$\nabla_r f^0 = \frac{\partial f^0}{\partial E_k}\left[-\nabla\mu - \frac{E_K-\mu}{T}\nabla T\right] \tag{2.41}$$

Furthermore

$$\nabla_k f^0 = \hbar v_k \frac{\partial f^0}{\partial E_k} \tag{2.42}$$

From equation 2.38, we substitute the relevant terms and retain only the second-order terms in the electric field, disregarding any terms involving the product of $g_k.E$.

$$-\frac{\partial f^0}{\partial E_k}.v_k.\left[-\frac{(E_k-\mu)}{T}\nabla T + eE - \nabla\mu\right] \tag{2.43}$$

$$= -\left.\frac{\partial f}{\partial t}\right|_{scattering} + v_k.\nabla_r g_k + \frac{e}{\hbar}(\mathbf{v_k}\times\mathbf{B}).\nabla_k g_k \tag{2.44}$$

The equation 2.44 derived is known as the Boltzmann transport equation. This equation can be used to derive expressions that describe the transport properties of a material.

In this research work, the thermoelectric transport properties, including electronic thermal conductivity, electrical conductivity and Seebeck coefficient of the PG were evaluated using Boltzmann transport theory. The self-consistent field (SCF) computed by density functional theory for PG was used as input and the electron transport properties were calculated using the semi-classical Boltzmann transport theory within the constant relaxation time approximation (CRTA) approach, as implemented in the BoltzTraP code. The BoltzTraP code was employed to calculate the thermoelectric properties mentioned above based on the SCF results. In the context of semi-classical transport theory, the transport tensors that correspond to the Seebeck coefficient ($S_{\alpha\beta}(T,\mu)$), electrical conductivity ($\sigma_{\alpha\beta}(T,\mu)$) and electronic

thermal conductivity ($\kappa_{\alpha\beta}(T,\mu)$) are formulated as (Madsen & Singh, 2006)

$$S_{\alpha\beta}(T,\mu) = \frac{1}{e\Omega T\,\sigma_{\alpha\beta}(T,\mu)} \int \sigma_{\alpha\beta}(\varepsilon)(\varepsilon-\mu)[\frac{-\partial f_0(T,\varepsilon,\mu)}{\partial\varepsilon}]d\varepsilon \tag{2.45}$$

$$\sigma_{\alpha\beta}(T,\mu) = \frac{1}{\Omega} \int \sigma_{\alpha\beta}(\varepsilon)[\frac{-\partial f_0(T,\varepsilon,\mu)}{\partial\varepsilon}]d\varepsilon \tag{2.46}$$

$$\kappa_{\alpha\beta}(T,\mu) = \frac{1}{e^2\Omega T} \int \sigma_{\alpha\beta}(\varepsilon)(\varepsilon-\mu)^2[\frac{-\partial f_0(T,\varepsilon,\mu)}{\partial\varepsilon}]d\varepsilon \tag{2.47}$$

The elements of the transport distribution tensor, represented by $\sigma_{\alpha\beta}$, are calculated by using Fourier interpolation on the band structure data. The indices α and β denote the tensor components. The variables Ω, μ, f_0 and T correspond to the cell volume, chemical potential, Fermi distribution function and absolute temperature, respectively. The self-consistent field (SCF) data is the required input to run the BoltzTraP algorithm.

3. METHODOLOGY

3.1. Overview of the research methodology

This chapter details the methodology utilized in the research, which comprises three primary components: NEMD for computing K_p, the Boltzmann transport equation for calculating K_e, electric conductivity and Seebeck coefficient; and the employment of specific software tools, namely LAMMPS and Boltztrap code.

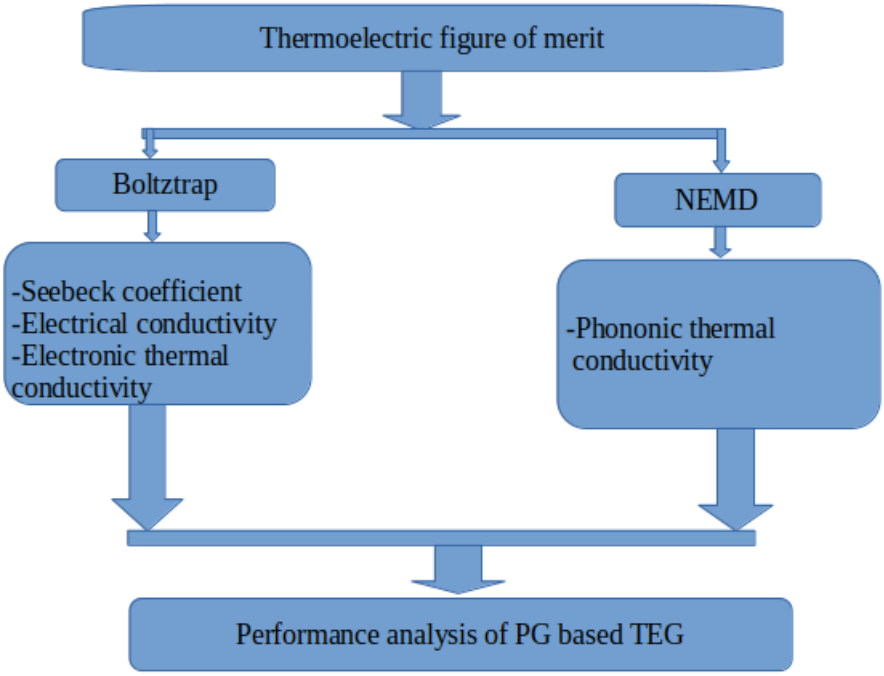

Figure 3.1: Methodology flowchart

3.2. Non equilibrium molecular dynamics simulation

To calculate K_p of PG, we employed NEMD. Our simulation utilized three-dimensional 10 x 10 x 1 unit cells containing 600 atoms. For the x and y directions, we applied periodic boundary conditions, while for the z direction, we implemented a non-periodic shrink-wrapped approach considering PG's two-dimensional nature. The forces between atoms were described using the Tersoff potential. To create distinct hot and cold regions, we utilized the Langevin thermostat.

As illustrates in Figure 3.2 the K_p of PG at a temperature of 150 K was determined through a three-stage simulation process. Additional information regarding the calculations can be found in the Appendix. The same stages were followed for evaluating the K_p at other temperature values. Random number generation was used to assign velocities to the atoms in the system. We examined six different temperatures, with the temperature change $\Delta T = (T_{higher} + T_{lower})/2$ being proportional to T (refer to Table 3.1 for specific values). The K_p of PG is calculated by using Fourier's Law equation 2.16.

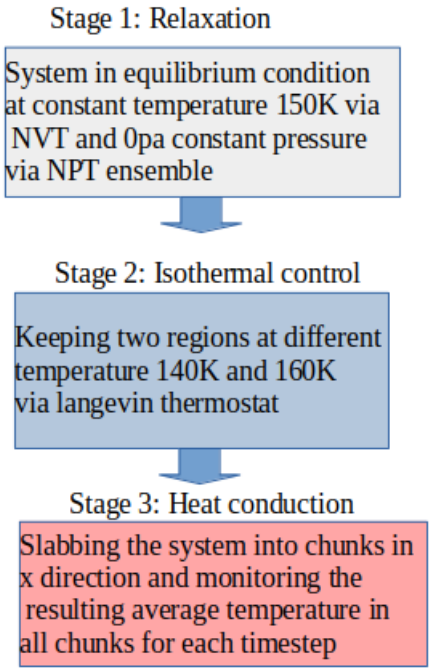

Figure 3.2: The three stages of performing NEMD simulation of heat transport at temperature 150K (Muna & Winczewski, 2020)

.

Temperature T (K)	Change of Temperature ΔT (K)	Tlo (K)	Thi (K)
150	10	140	160
300	20	280	320
450	30	420	480
600	40	560	640
750	50	700	800
900	60	840	960

Table 3.1: Specification of temperatures used to investigate phonon thermal conductivity of PG

.

3.3. Boltzmann transport equation

We conducted calculations for thermoelectric properties including electronic thermal conductivity, electric conductivity and Seebeck coefficient for PG using Boltztrap code. Our calculations were based on the semi-classical Boltzmann theory and the constant relaxation time (τ) approximation, which allows for the Seebeck coefficient to remain independent of τ, while the electrical conductivity and electronic thermal conductivity are calculated with respect to τ (Madsen & Singh, 2006). The electron relaxation time, representing the duration for electrons to restore equilibrium after perturbation in PG, is expressed by equation 3.1 (Chen et al., 2017).

$$\tau = \frac{2\hbar^3}{3k_B T m^* E_{DP}^2} \tag{3.1}$$

Where the parameter m^* is the density of state effective mass along the kx and ky directions. In addition, $\hbar$ and k_B are the reduced Planck constant and the Boltzmann constant, C is the elastic constant and E_{DP} is the deformation potential constant.

To calculate the conductivity, knowledge of the relaxation time is essential. Therefore, we determined the relaxation time at various temperature values using equation 3.1 (Chen et al., 2017). The resulting relaxation times were then multiplied by the values obtained from Boltztrap code, representing the electric conductivity and electronic thermal conductivity per relaxation time denoted as σ/τ and K_e/τ respectively. Table 3.2 displays the respective values for reference.

Temperature T (K)	Electron τ (ps) in PG
150	0.240
300	0.120
450	0.080
600	0.060
750	0.048
900	0.040

Table 3.2: Electron relaxation time of PG at different temperature

.

3.4. Software requirement

In this research work, a diverse range of software packages was utilized. LAMMPS was employed for calculating the K_p of PG, while Python2 was used in conjunction with the Boltztrap code to obtain the K_e, seebeck coefficient and electric conductivity. LaTeX was utilized for documenting the research findings, Gnuplot served as the tool for generating graphical plots, vesta and other associated software tools were also incorporated throughout the study.

4. RESULTS AND DISCUSSIONS

4.1. Overview

This chapter presents the results and discussions of the research work, focusing on key parameters that influence the performance of the TEG based on PG. The study specifically analyzes the K_p, which governs heat transfer through lattice vibrations and the electronic thermal conductivity, which pertains to heat transfer through electrons. Additionally, the power factor, a critical metric obtained by squaring the Seebeck coefficient and multiplying it by the electrical conductivity, is thoroughly discussed. The performance of the PG-based TEG is evaluated by considering the combined effects of K_p and K_e, as well as the power factor. These results offer valuable insights into the potential of PG as an efficient TEM for energy harvesting applications. Finally, the performance of the PG based TEG is assessed at different temperature differentials between the hot and cold sides, employing the ZT.

4.2. Phonon thermal conductivity

Phonon thermal conductivity plays a critical role in determining the performance of TEGs. Research findings demonstrate that PG, a TEM, exhibits an exceptionally low K_p when compared to graphene, showcasing its promising potential for TEG. This low K_p of PG suggests its effective impeding of heat transfer through lattice vibrations, resulting in reduced heat dissipation, preserved temperature differences and maximized thermoelectric conversion efficiency (Radouane, 2023).

Prior research has shown varying projections for the room temperature K_p of PG. In 2016, reported a significantly lower value of approximately 645 W/mK compared to graphene (Wang et al., 2016), while in 2015, estimated a K_p of about 167 W/mK (Xu et al., 2015). Additionally, in 2020, predicted an even lower value of around 18 W/mK for PG (Muna & Winczewski, 2020). In this study, we obtained the K_p of PG at room temperature (300 K) to be 26 W/mK, which aligns with the result of Muna & Winczewski (2020) which is much lower than that of graphene and higher than phonon thermal conductivity of $CuFeS_2$ and several state-of-the-art TEM, such as Bi_2Te_3, PbTe and SiGe, as well as sulfide materials

like TiS_2, PbS, $CuFeS_2$, $Cu_{12}Sb_4S_{13}$ and Cu_2S (Qiu et al., 2014).

Our study shows that there is a declining trend in the thermal conductivity of PG as the temperature rises, which is consistent with previous research findings. This trend is illustrated in Figure 4.1. The reduction in thermal conductivity with increasing temperature is advantageous for TEG because it allows for better heat retention within the material, minimizing heat dissipation and maximizing the temperature difference between the hot and cold sides of the generator. This temperature-dependent behavior enhances the TEG conversion efficiency, enabling the efficient conversion of a larger temperature gradient into electrical energy, which is beneficial for the overall performance of the TEG.

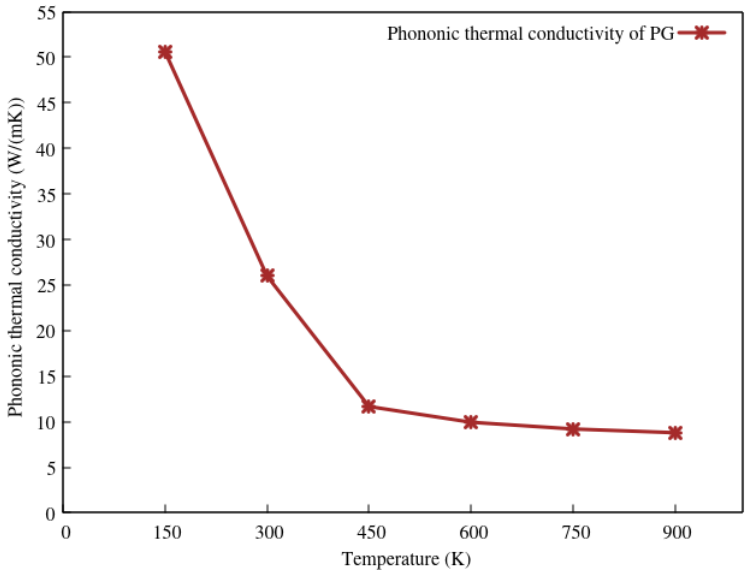

Figure 4.1: K_p of PG as a function of temperature

The thermal conductivity of phonons in PG follows a similar pattern as that of graphene (Gu & Yang, 2016), although the latter exhibits a higher trend. The thermal conductivity of phonons in PG decreases significantly from 150K to 450K, indicating that phonons are scatter efficiently up to 450K. Beyond this temperature, their scattering becomes less effective and they only show slight scattering. This increased scattering reduces the ability of phonons to transport heat efficiently, resulting in the observed decline in phonon thermal conductivity. At even higher temperatures (above 450K), the rate of phonon scattering continues to increase, but its effect on phonon thermal conductivity becomes less pronounced.

4.3. Electronic thermal conductivity

The TEM's ability to transfer heat through electron movement demonstrates that PG, in its role as a TEM, has a relatively lower thermal conductivity due to electrons (K_e) compared to its thermal conductivity due to phonons (K_p), which contributes to its performance in TEGs. The lower K_e suggests PG has limited heat transport capability through electrons, making it suitable for TEGs, as minimizing electronic heat conduction allows PG to efficiently convert waste heat into usable electrical energy. As shown in figure 4.2 the electronic thermal conductivity of PG increases linearly with temperature, similar to graphene (Abbood & Jabour, 2017) but with a higher value and this increasing K_e as a function of temperature has a negative impact by maximizing heat dissipation and minimizing the temperature difference between the hot and cold sides of the TEG, leading to a reduction in voltage output and efficiency.

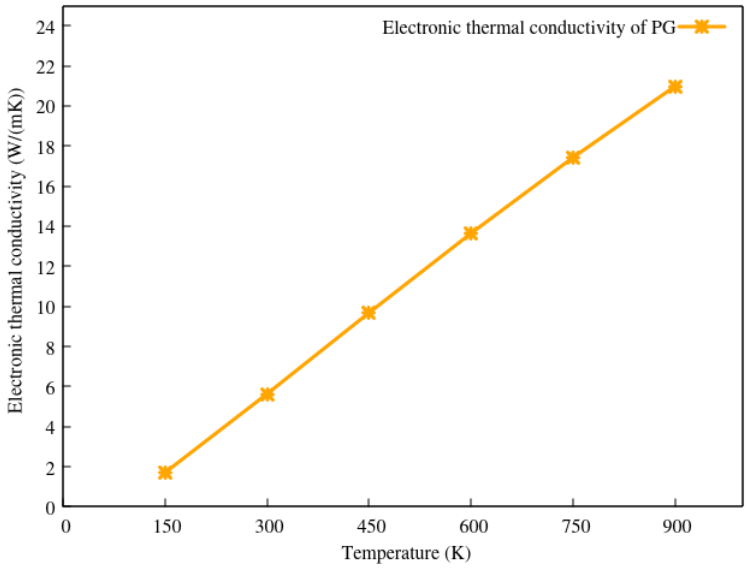

Figure 4.2: Electronic thermal conductivity of PG as function of temperature

4.4. Electric conductivity

As shown in the figure 4.3 the electric conductivity of PG increases with rising temperature. This property of TEM in TEG is advantageous, as it enables efficient electron movement and results in increased power output for a given temperature gradient. As temperature increases, the material's electrical conductivity also increases, allowing for more efficient flow of electric current. This temperature-dependent behavior enhances the con-

version of heat into electricity, making PG well-suited for harnessing waste heat into useful electrical energy.

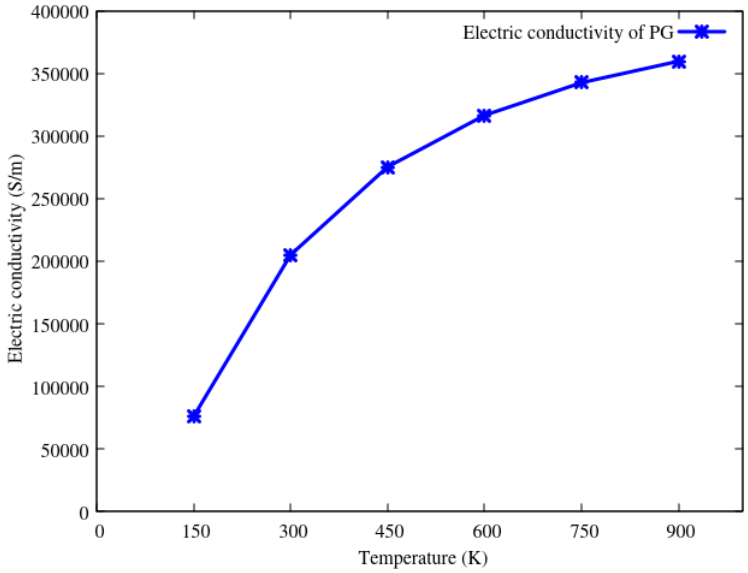

Figure 4.3: Electric conductivity of PG as function of temperature

.

As the temperature increases, the rate of increase in electrical conductivity of PG actually decreases. This is because as the temperature goes up, the electron relaxation time within PG decreases. In other words, the electrons in PG have less time to relax between collisions as the temperature rises. This increased electron scattering due to the higher temperature can ultimately reduce the electrical conductivity of the material.

4.5. Seebeck coefficient

The graph show the Seebeck coefficient of PG as a function of temperature reveals an impressive Seebeck coefficient of 0.278 x 10^{-3} V/K at 300 K, which surpasses that of traditional TEM materials like Bi_2Te_3 with a Seebeck coefficient of 0.248 x 10^{-3} V/K (Kim et al., 2020). Previous studies on PG have reported a maximum Seebeck coefficient value of 3.671×10^{-3} V/K at room temperature (300 K) (Deb et al., 2022). This finding further emphasizes the potential of PG as a TEM for TEG. It is crucial to optimize the Seebeck coefficient of the TEM to efficiently convert waste heat into usable electrical energy and enhance the TEG.

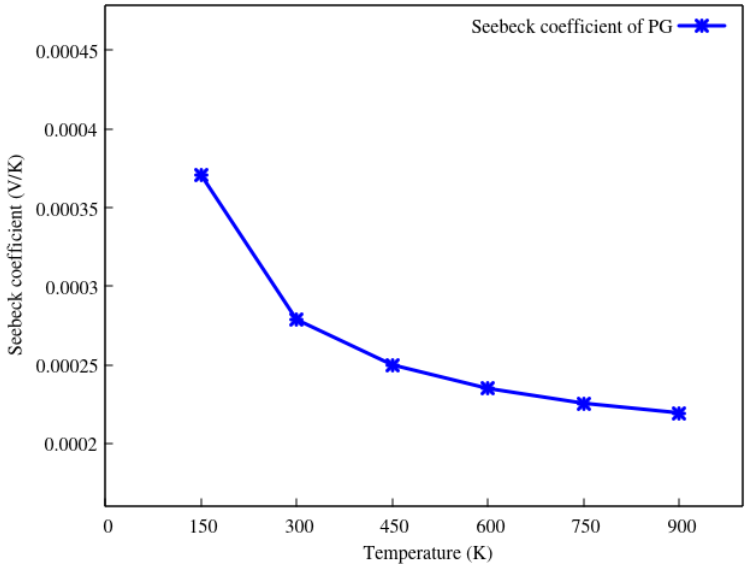

Figure 4.4: Seebeck coefficient of PG as function of temperature.

It is important to note that the Seebeck coefficient typically decreases as temperature rises, with the rate of decrease becoming slower as temperature increases. This results in a slight reduction in voltage generation when the temperature difference is significant. This phenomenon occurs because at low temperatures, phonon activity is minimal. Phonons are lattice vibrations that can obstruct electron flow by scattering them, reducing their mobility. With minimal phonon scattering, electrons can move more freely, resulting in a higher Seebeck coefficient. However, as temperature increases, thermal energy activates phonons, making them more prevalent. These phonons then hinder electron flow by scattering them more frequently, which in turn reduces the Seebeck coefficient. This behavior is demonstrated in Figure 4.4, which shows the temperature dependence of the Seebeck coefficient.

4.6. Power factor

The power factor is obtained by the product of the square of the Seebeck coefficient and the electrical conductivity plays a crucial role in assessing the efficiency of TEM, particularly in the context of TEG (W. Liu et al., 2016). Maintaining a high power factor is essential for optimizing generator performance by enabling efficient conversion of temperature gradients into electrical energy, thus minimizing power losses and maximizing overall system efficiency. The significant value of the Seebeck coefficient indicates its remarkable

ability to generate electric potential in response to a temperature gradient, while the relatively high electric conductivity of PG suggests efficient charge carrier transport.

The graph of Power factor of PG as a function of temperature in figure 4.5 shows an upward trajectory until 450 K, maintaining a consistent level beyond this temperature. These observations emphasize PG's effectiveness at 600 K and its potential for energy conversion in TEG. The power factor plays a significant role in the performance of a TEG, particularly in response to temperature changes. Up to 450 K, an enhanced power factor positively impacts the TEG's efficiency and power output. As the power factor increases, the TEG can more effectively convert a larger portion of the temperature gradient into electrical energy. However, beyond this temperature threshold, further improvements in power factor do not lead to substantial enhancements in TEG performance. Thus, maintaining an elevated power factor within the 600 K range is crucial for optimizing the efficiency and power output of a TEG, while adjusting the power factor beyond this temperature range does not yield notable benefits.

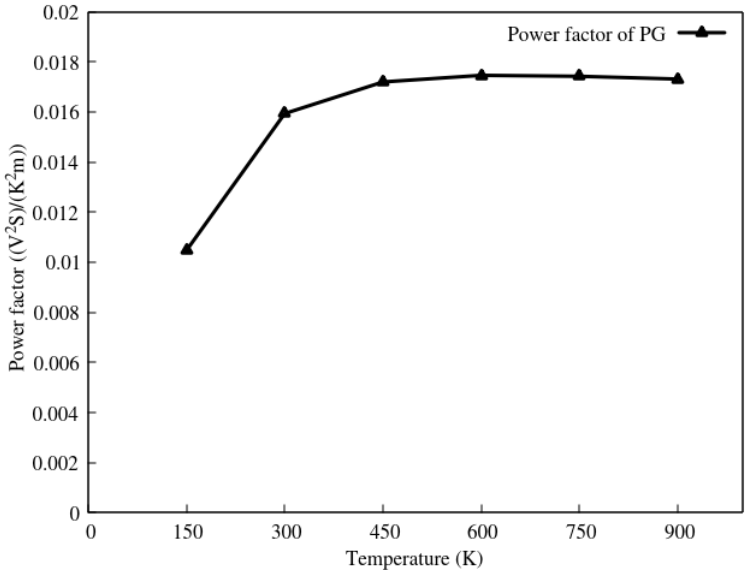

Figure 4.5: Power factor of PG as a function of temperature

As depicted in Figure 4.5, the power factor experiences a rise from 150K to 450K as a result of an increase in electrical conductivity, which dominates the process. Beyond the 450K mark, the power factor remains constant due to the diminishing rate of increase in electrical conductivity and diminishing rate of decreasing Seebeck coefficient as temperature rises.

4.7. Total thermal conductivity

The total thermal conductivity of a TEM obtained from addition of electronic and phonon contributions, representing its ability to conduct heat. It is a crucial parameter that significantly influences the performance of a TEG. In TEMs, a low thermal conductivity is desirable as it minimizes heat loss, enabling the establishment of a larger temperature gradient across the TEG. This temperature gradient is vital for generating a voltage difference and facilitating the flow of electrons, resulting in efficient conversion of heat into electrical energy (Radouane, 2023).

Our study shows that the K_p value of the PG diminishes as the temperature rises, as phonons take over as the primary thermal carriers at lower temperatures. On the other hand, K_e increases with temperature, since electrons become the dominant thermal carriers at higher temperatures. The graph depicting the total thermal conductivity of PG as a function of temperature exhibits a more rapid decrease from 150K to 450K and then slightly increases beyond 450K, as illustrated in Figure 4.6 this due to dominance of phonon in thermal energy carrying from 150K upto 450K and dominance of electron in thermal energy carrying from 450K upto 900K.

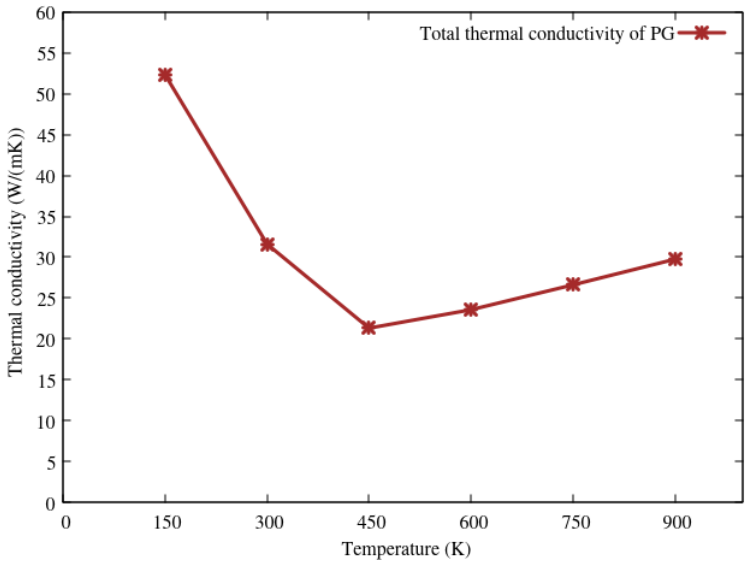

Figure 4.6: Total thermal conductivity of PG as a function of temperature

4.8. Thermoelectric figure of merit

Previous studies utilized the Atomistix ToolKit (ATK) software package to assess the ZT of PG using the generalized gradient approximation (GGA) with the Perdew-Burke-Ernzerhof (PBE) exchange-correlation functional (Deb et al., 2022). These studies reported a moderate ZT value of 0.14 for PG at 700 K. In this research by utilizing equation 2.15, we extended the investigation of PG's thermoelectric properties and found a ZT value of 0.45 at 700 K, indicating its potential for energy conversion in TEGs (Deb et al., 2022). The graph illustrating ZT of PG as a function of temperature indicates that at room temperature (300 K), a ZT value of 0.15 is obtained for PG, which is 16.6 times higher than that of graphene (Chen et al., 2017). Despite this, PG's ZT is lower than that of well-established TEMs, such as Bi_2Te_3 at low temperature range and PbTe at medium temperatures, which are widely regarded as top-performing TEMs (Snyder & Toberer, 2008). Notably, we observed that PG's ZT value increased with temperature, as depicted in Figure 4.7. This temperature-dependent enhancement implies that PG can effectively utilize significant temperature differences, making it a promising candidate for TEGs. ZT from 300K to 450 highly increased thermal conductivity is low between these temperature. Furthermore, PG exhibits good stability at medium temperature ranges and can withstand temperatures as high as 1000 K (Zhang et al., 2015).

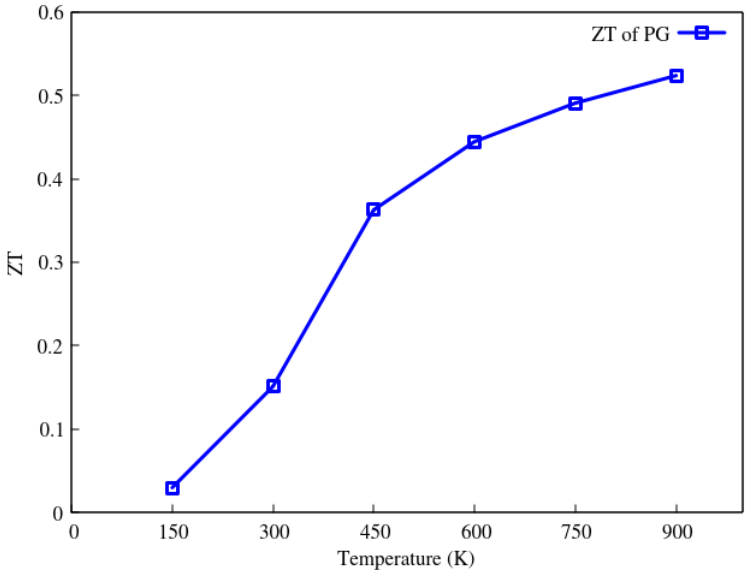

Figure 4.7: ZT of PG as a function of temperature.

The simulation study demonstrates the potential of PG as a TEM for energy conversion in TEGs. Its higher ZT values at both room temperature and elevated temperatures, along

with its ability to utilize large temperature differences, make it a promising candidate for further exploration and development in the field of thermoelectric energy harvesting.

4.9. Efficiency of PG based TEG

The efficiency of a TEG is a crucial factor that determines its ability to convert heat energy into electrical energy. The efficiency of a TEG is affected by various factors, such as the thermoelectric properties of the materials used and the temperature difference. In this study, we focused on analyzing the efficiency of a PG based TEG using equation 1.1, and we considered an average ZT of PG with a value of 0.337. We determined the efficiency of the TEG when operating at a hot side temperature of 900K and a cold side temperature of 300K. Our simulation results showed a maximum efficiency of 0.0698, equivalent to 6.98%. This value positions the PG based TEG as intermediate in terms of efficiency compared to other sources (Hu et al., 2016). It is important to note that smaller temperature differences lead to decreased efficiency.

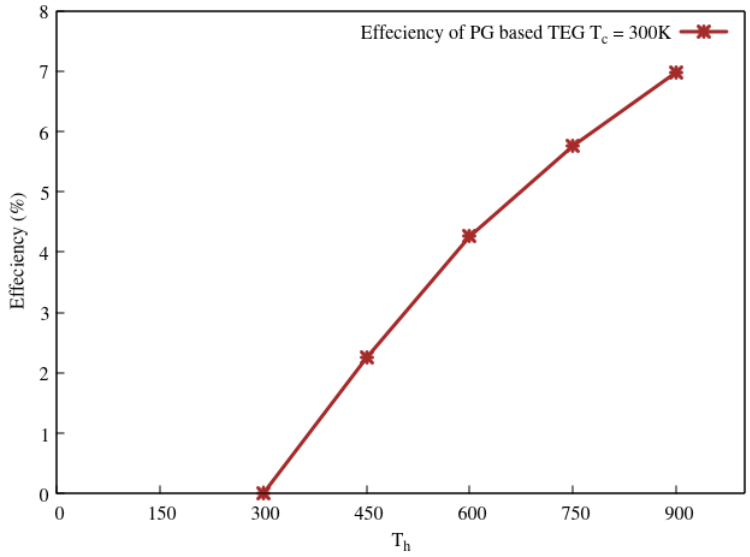

Figure 4.8: Performance of PG-based TEG

Furthermore, our analysis investigated the impact of varying temperature differences on the efficiency of the PG based TEG. We maintained a constant temperature of 300K on the cold side while gradually increasing the temperature of the hot side (T_h), as depicted in Figure 4.8. Through this investigation, we observed an upward trend with decreasing rate because of decreasing in average ZT in the efficiency of the PG based TEG with increased

temperature differences. This finding highlights the good efficiency of PG as an organic TEM, which falls under the category of carbon-based materials. These materials hold significant potential for the development of flexible and wearable self-powered devices, an area currently lacking in the market but extensively researched.

Organic TEMs offer advantages over traditional chalcogenides like bismuth telluride, including nontoxic, lower cost, greater availability on Earth and intrinsic flexibility. Moreover, they exhibit high thermoelectric performance around room temperature, making them particularly suitable for addressing the growing demand for wearable and flexible devices driven by the IoT. While achieving high thermoelectric efficiency remains a challenge, our findings demonstrate the effectiveness of PG based TEG, even at temperatures above room temperature, with a ZT of 0.52 at 900K, highly performing polymeric materials that typically reach ZT values no higher than 0.75 that obtained at 300K (Fan et al., 2018).

5. CONCLUSIONS AND RECOMMENDATIONS

5.1. Conclusions

In this study, we analyzed the performance of PG-based TEGs through simulation. NEMD simulations with the LAMMPS simulator revealed that PG has a K_p of 26 W/(mK) at room temperature lower than graphene with a decreasing trend as temperature increases. Using the Boltzmann transport equation in the Boltztrap code, we calculated the electronic thermal conductivity, electric conductivity and Seebeck coefficient of PG. Evaluating TEG performance at various temperatures, we found that the ZT of PG increases with temperature reaching 0.52 at 900K indicating its intermediate ZT compared to other TEMs. Varying the hot side temperature while keeping the cold side constant at 300K, the efficiency of the PG-based TEG reached 7% at T_h = 900K. PG as an organic TEM offers advantages over traditional chalcogenides, including cost-effectiveness, availability and flexibility. With high thermoelectric performance, including a ZT of 0.15 around room temperature, 16 times that of graphene, PG is suitable for wearable and flexible devices in the IoT era. Despite challenges in achieving high thermoelectric efficiency, PG-based TEGs demonstrate effectiveness even at temperatures above room temperature. Distinguished from other organic TEMs, PG-based TEGs excel at medium-temperature range, presenting opportunities for the development of flexible and self-powered devices.

5.2. Recommendations

According to the analysis of PG-based TEG's performance, PG exhibits good performance as an organic TEM. However, when compared to chalcogenides and some other type of TEM's it falls intermediate. Given this, we encourage researchers to continue exploring strategies for improving the thermoelectric performance of organic TEMs, which are currently underdeveloped in the market. By focusing on enhancing the ZT and efficiency of PG-based TEGs, it is possible to advance their development and meet the increasing demands for wearable and self-powered devices, especially in the age of IoT.

Research Fund Acknowledgment

This Research Project is funded by Adama Science and Technology University under the grant number ASTU/SM-R/987/24, Adama, Ethiopia.

References

Abbood, H. I., & Jabour, H. S. (2017). Theoretical study of electronic and electrical properties of pure and doped graphene sheets. *International Journal of Advanced Engineering Research and Science*, *4*(7), 237220.

Allen, & P, M. (2004). Introduction to molecular dynamics simulation. *Computational soft matter: from synthetic polymers to proteins*, *23*(1), 1–28.

Baranowski, L. L., Jeffrey Snyder, G., & Toberer, E. S. (2013). Effective thermal conductivity in thermoelectric materials. *Journal of Applied Physics*, *113*(20).

Beltrán-Pitarch, B., Prado-Gonjal, J., Powell, A. V., Ziolkowski, P., & García-Cañadas, J. (2018). Thermal conductivity, electrical resistivity, and dimensionless figure of merit (zt) determination of thermoelectric materials by impedance spectroscopy up to 250 c. *Journal of Applied Physics*, *124*(2).

Cai, Y., Xiao, J., Zhao, W., Tang, X., & Zhang, Q. (2011). A general model for the electric power and energy efficiency of a solar thermoelectric generator. *Journal of electronic materials*, *40*, 1238–1243.

Champier, D. (2017). Thermoelectric generators: A review of applications. *Energy Conversion and Management*, *140*, 167–181.

Chen, C.-P., Liu, C., Liu, L.-L., Zhao, L.-S., & Wang, X.-C. (2017). Enhanced thermoelectric properties of penta-graphene by strain effects process. *Materials Research Express*, *4*(10), 105031.

Deb, J., Mondal, R., Mukherjee, S., & Sarkar, U. (2022). Thermoelectric properties of pentagraphene. *Physica B: Condensed Matter*, *641*, 414091.

De Sousa, J., Aguiar, A., Girão, E., Fonseca, A. F., Souza Filho, A., & Galvão, D. (2021). Computational study of elastic, structural stability and dynamics properties of penta-graphene membrane. *Chemical physics*, *542*, 111052.

Dror, R. O., Dirks, R. M., Grossman, J., Xu, H., & Shaw, D. E. (2012). Biomolecular simulation: a computational microscope for molecular biology. *Annual review of biophysics*, *41*, 429–452.

Dunham, M. T., Hendricks, T. J., & Goodson, K. E. (2019). Thermoelectric generators: A case study in multi-scale thermal engineering design. , *51*, 299–350.

d'Angelo, M., Galassi, C., & Lecis, N. (2023). Thermoelectric materials and applications: A review. *Energies*, *16*(17), 6409.

Eivari, H. A., Sohbatzadeh, Z., Mele, P., & Assadi, M. (2021). Low thermal conductivity: Fundamentals and theoretical aspects in thermoelectric applications. *Materials Today Energy*, *21*, 100744.

Elsheikh, M. H., Shnawah, D. A., Sabri, M. F. M., Said, S. B. M., Hassan, M. H., Bashir, M. B. A., & Mohamad, M. (2014). A review on thermoelectric renewable energy: Principle parameters that affect their performance. *Renewable and sustainable energy reviews*, *30*, 337–355.

Ercolessi, F. (1997). A molecular dynamics primer. *Spring college in computational physics, ICTP, Trieste*, *19*.

Erhart, P., & Albe, K. (2005). Analytical potential for atomistic simulations of silicon, carbon, and silicon carbide. *Physical Review B*, *71*(3), 035211.

Fan, Z., Du, D., Guan, X., & Ouyang, J. (2018). Polymer films with ultrahigh thermoelectric properties arising from significant seebeck coefficient enhancement by ion accumulation on surface. *Nano energy*, *51*, 481–488.

Gu, X., & Yang, R. (2016). Phonon transport and thermal conductivity in two-dimensional materials. *Annual review of heat transfer*, *19*.

He, W., Zhang, G., Zhang, X., Ji, J., Li, G., & Zhao, X. (2015). Recent development and application of thermoelectric generator and cooler. *Applied Energy*, *143*, 1–25.

Hospital, A., Goñi, J. R., Orozco, M., & Gelpí, J. L. (2015). Molecular dynamics simulations: advances and applications. *Advances and Applications in Bioinformatics and Chemistry*, 37–47.

Hu, X., Jood, P., Ohta, M., Kunii, M., Nagase, K., Nishiate, H., & Kanatzidis. (2016). Power generation from nanostructured pbte-based thermoelectrics: comprehensive development from materials to modules. *Energy & Environmental Science*, *9*(2), 517–529.

Jaziri, N., Boughamoura, A., Müller, J., Mezghani, B., Tounsi, F., & Ismail, M. (2020). A comprehensive review of thermoelectric generators: Technologies and common applications. *Energy reports*, *6*, 264–287.

Juárez-Huerta, V., Sánchez-Salas, N., & Chimal-Eguía, J. (2022). Optimization criteria and efficiency of a thermoelectric generator. *Entropy*, *24*(12), 1812.

Karamitaheri, H. (2013). Thermal and thermoelectric properties of nanostructures. *TU Wien*, 1–2.

Kim, D., Du, R., Yu, S.-Y., Yin, Y., Dong, S., Li, Q., & Mohney. (2020). Enhanced thermoelectric efficiency in nanocrystalline bismuth telluride nanotubes. *Nanotechnology*, *31*(36), 365703.

LeBlanc, S. (2014). Thermoelectric generators: Linking material properties and systems engineering for waste heat recovery applications. *Sustainable Materials and Technologies*, *1*, 26–35.

Lesage, F. J., & Pagé-Potvin, N. (2013). Experimental analysis of peak power output of a thermoelectric liquid-to-liquid generator under an increasing electrical load resistance. *Energy conversion and management*, *66*, 98–105.

Li, G., Ma, X., Shittu, S., & Zhao, X. (2019). Solar thermoelectric technologies for power generation. *Advanced Energy Efficiency Technologies for Solar Heating, Cooling and Power Generation*, 341–371.

Liu, I.-S. (1990). On fourier's law of heat conduction. *Continuum mechanics and Thermodynamics*, *2*, 301–305.

Liu, W., Kim, H. S., Jie, Q., & Ren, Z. (2016). Importance of high power factor in thermoelectric materials for power generation application: A perspective. *Scripta Materialia*, *111*, 3–9.

Madsen, G. K., & Singh, D. J. (2006). Boltztrap. a code for calculating band-structure dependent quantities. *Computer Physics Communications*, *175*(1), 67–71.

Mamur, H., & Ahıska, R. (2014). A review: Thermoelectric generators in renewable energy. *International journal of renewable energy research*, *4*(1), 128–136.

Mary-Rose, M., & WallenfeldtAn, J. (2024). Thermoelectric power generator. *Encyclopædia Britannica, Inc.*, 1.

Meng, J.-H., Zhang, X.-X., & Wang, X.-D. (2015). Characteristics analysis and parametric study of a thermoelectric generator by considering variable material properties and heat losses. *International journal of heat and mass transfer*, *80*, 227–235.

Muna, I. I., & Winczewski, S. (2020). Molecular dynamics simulations of thermal conductivity of penta-graphene. *TASK Quarterly*, *24*, 191–220.

Qiu, P., Zhang, T., Qiu, Y., Shi, X., & Chen, L. (2014). Sulfide bornite thermoelectric material: a natural mineral with ultralow thermal conductivity. *Energy & Environmental Science*, *7*(12), 4000–4006.

Radouane, N. (2023). Thermoelectric generators and their applications: Progress, challenges, and future prospects. *Chinese Physics B*, *32*(5), 057307.

Ramasubramanian, B., Sundarrajan, S., Rao, R. P., Reddy, M., Chellappan, V., & Ramakrishna, S. (2022). Novel low-carbon energy solutions for powering emerging wearables, smart textiles, and medical devices. *Energy & Environmental Science*, *15*(12), 4928–4981.

Rowe, D. (1978). Thermoelectric power generation. In *Proceedings of the institution of electrical engineers* (Vol. 125, pp. 1113–1136).

Singh, B., Baharin, N. Remeli, M. F., Oberoi, A., Date, A., & Akbarzadeh, A. (2017). Experimental analysis of thermoelectric heat exchanger for power generation from salinity gradient solar pond using low-grade heat. *Journal of Electronic Materials*, *46*, 2854–2859.

Singh, B. S. B. (2023). Thermoelectric generators: Design, operation, and applications. *New Materials and Devices for Thermoelectric Power Generation*, 1–14.

Singh, J. (2008). Modern physics for engineers. *Wiley-VCH*, *16*, 353–363.

Snyder, G. J., & Snyder, A. H. (2017). Figure of merit zt of a thermoelectric device defined from materials properties. *Energy & Environmental Science*, *10*(11), 2280–2283.

Snyder, G. J., & Toberer, E. S. (2008). Complex thermoelectric materials. *Nature materials*, *7*(2), 105–114.

Sun, Y., Liu, Y., Li, R., Li, Y., & Bai, S. (2022). Strategies to improve the thermoelectric figure of merit in thermoelectric functional materials. *Frontiers in Chemistry*, *10*, 865281.

Tersoff, J. (1989). Modeling solid-state chemistry: Interatomic potentials for multicomponent systems. *Physical review B*, *39*(8), 5566.

Tundee, S., Srihajong, N., & Charmongkolpradit, S. (2014). Electric power generation from solar pond using combination of thermosyphon and thermoelectric modules. *Energy Procedia*, *48*, 453–463.

Wang, F. Q., Yu, J., Wang, Q., Kawazoe, Y., & Jena, P. (2016). Lattice thermal conductivity of penta-graphene. *Carbon*, *105*, 424–429.

Xu, W., Zhang, G., & Li, B. (2015). Thermal conductivity of penta-graphene from molecular dynamics study. *The Journal of chemical physics*, *143*(15).

Zhang, S., Zhou, J., Wang, Q., Chen, X., Kawazoe, Y., & Jena, P. (2015). Penta-graphene: A new carbon allotrope. *Proceedings of the National Academy of Sciences*, *112*(8), 2372–2377.

Zide, J., Vashaee, D., Bian, Z., Zeng, G., Bowers, J., Shakouri, A., & Gossard, A. (2006). Demonstration of electron filtering to increase the seebeck coefficient in in 0.53 ga 0.47 as/ in 0.53 ga 0.28 al 0.19 as superlattices. *Physical Review B*, *74*(20), 205335.

Appendices

```
# LAMMPS input script for calculating phonon thermal conductivity of PG
# Thermostatting 2 regions via fix langevin


# Settings
dimension 3
boundary p p m
units metal
atom_style atomic


# Variables
variable kB equal 0.00008617
variable t equal 150
variable tlo equal 140
variable thi equal 160


# Setup problem
read data pentaopt10X10X1.lammps-data
mass 1 12.0


# Interatomic potential
pair_style tersoff
pair_coeff * * SiC_Erhart-Albe.tersoff C


# Adjusted timestep value
timestep 0.0005
```

```
        # Heat layers
region    hot block 0 12.13 INF INF INF INF
region    cold block 24.26 36.403995999999999 INF INF INF INF
velocity     all create 150 87287
Cobalt compute     Thot all temp/region hot
compute     Tcold all temp/region cold


        # 1st equilibration run
# NPT (constant Number of particles, Pressure and Temperature) equilibration
fix     1 all npt temp 150 150 1.0
x 0.0 0.0 1.0
y 0.0 0.0 1.0
couple none
thermo_style     custom step temp press lx ly
thermo     100
run     1000
velocity     all scale 300
unfix     1
# NVT (constant Number of particles, Volume and Temperature) equilibration
fix     1 all nvt temp 150 150 0.1
thermo_style     custom step temp pe etotal press vol
thermo     100
run     1000
velocity     all scale 150
unfix     1


        # 2nd equilibration run
# NVE (constant Number of particles, Volume and Energy) equilibration
fix     1 all nve
fix     hot all langevin 160 160 0.2 59804 tally yes
fix     cold all langevin 140 140 0.2 287859 tally yes
```

```
fix_modify      hot temp Thot
fix_modify      cold temp Tcold
variable      tdiff equal c_Thot-c_Tcold
thermo_style      custom step temp c_Thot c_Tcold f_hot f_cold v_tdiff
thermo      1000
run      10000


        # Thermal conductivity calculation
compute      ke all ke/atom
variable      temp atom c_ke/(1.5 * kB)
fix      hot all langevin 160 160 0.2 59804 tally yes
fix      cold all langevin 140 140 0.2 287859 tally yes
fix modify      hot temp Thot
fix modify      cold temp Tcold
fix      ave all ave/time 10 100 1000 v_tdiff ave running
thermo_style      custom step temp c_Thot c_Tcold f_hot f_cold v_tdiff f_ave
compute      layers all chunk/atom bin/1d x lower 0.05 units reduced
fix      2 all ave/chunk 10 100 1000 layers v_temp file profile.langevin
variable      start-time equal time
variable      kappa equal (0.5*(abs(f_hot)+abs(f_cold))/(time - start time)/(lz*ly))*(lx)/f_ave
run      20000
print      "Running average thermal conductivity metal unit style: $(v_kappa:%.5f)"
print      "Running average thermal conductivity W/mK: $(v_kappa*1.60218e+3:%.5f)"
```